iScience

Article

Cab45G trafficking through the insulin secretory pathway is altered in human type 2 diabetes

Graphical abstract

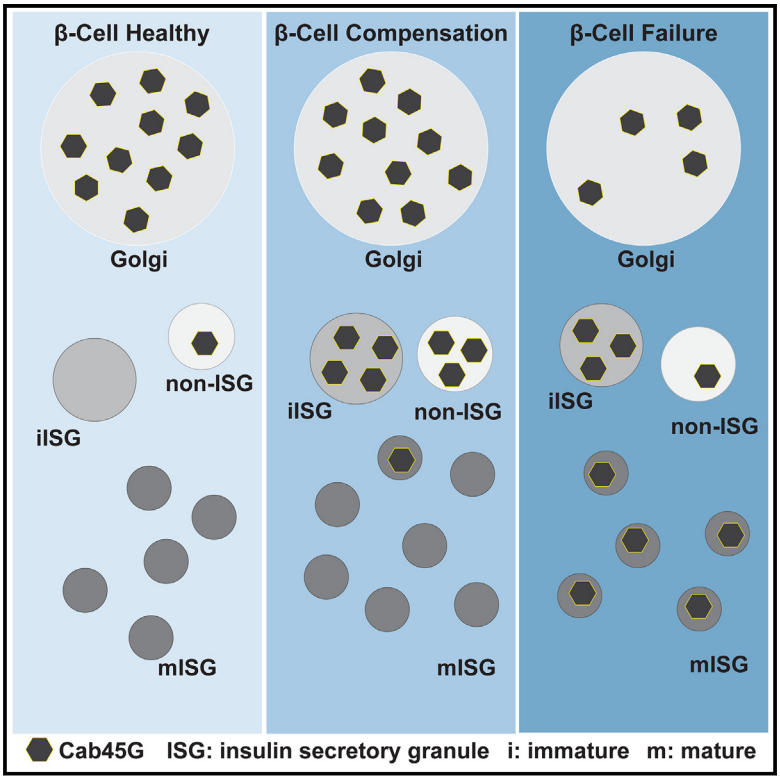

Authors

Mark Germanos, Belinda Yau, Matthew Taper, ..., Michael Ailion, Cedric Asensio, Melkam Alamerew Kebede

Correspondence

melkam.kebede@sydney.edu.au

In brief

Biological sciences; Cell biology; Organizational aspects of cell biology; Specialized functions of cells; Functional aspects of cell biology

Highlights

- Cab45G is Golgi-localized in β-cells but can traffic anterograde into vesicles
- Cab45G loss affects Ca^{2+} homeostasis and causes a secretory defect in INS1 cells
- Cab45G overexpression stimulates granule production in INS1 cells
- Obesity increases Cab45G trafficking and Golgi-localized Cab45G is lost in T2D

Germanos et al., 2025, iScience *28*, 111719
February 21, 2025
https://doi.org/10.1016/j.isci.2024.111719

CellPress

iScience

CellPress
OPEN ACCESS

Article

Cab45G trafficking through the insulin secretory pathway is altered in human type 2 diabetes

Mark Germanos,[1,7] Belinda Yau,[1,7] Matthew Taper,[1] Cara Yeoman,[1] Amy Wilson,[1] Yousun An,[1] Jerome Cattin-Ortolá,[2] Drew Masler,[3] Jason Tong,[1] Sheyda Naghiloo,[1] Elise J Needham,[4] A Gabrielle van der Kraan,[1] Kitty Sun,[1] Thomas Loudovaris,[5] Alexis Diaz-Vegas,[4] Mark Larance,[1] Helen Thomas,[5] Helen von Blume,[6] Peter Thorn,[1] Michael Ailion,[2] Cedric Asensio,[3] and Melkam Alamerew Kebede[1,8,*]

[1]School of Medical Sciences, Charles Perkins Centre, The University of Sydney, Camperdown, NSW, Australia
[2]Department of Biochemistry, University of Washington, Seattle, WA, USA
[3]Department of Biological Sciences, University of Denver, Denver, CO 80210, USA
[4]School of Life and Environmental Sciences, Charles Perkins Centre, The University of Sydney, Camperdown, NSW, Australia
[5]Immunology and Diabetes Unit, St Vincent's Institute, Department of Medicine, St Vincent's Hospital, University of Melbourne, Fitzroy, VIC 3065, Australia
[6]Department of Cell Biology, Yale University School of Medicine, New Haven, CT 06510, USA
[7]These authors contributed equally
[8]Lead contact
*Correspondence: melkam.kebede@sydney.edu.au
https://doi.org/10.1016/j.isci.2024.111719

SUMMARY

In type 2 diabetes (T2D), the rate of insulin secretory granule biogenesis can limit insulin secretion from pancreatic β-cells. Using rat insulinoma INS1 β-cells, we show that the soluble Ca^{2+}-binding/trafficking protein, Cab45G, serves as a non-essential chaperone for insulin granule biogenesis. In β-cells, Cab45G is stored within a *cis*-Golgi reservoir. Cab45G deletion dysregulates Ca^{2+} homeostasis and leads to secretory abnormality, but insulin granule biogenesis remains intact. Increasing Cab45G biosynthesis leads to anterograde trafficking into insulin granules, stimulating their production. Using human donor islets, we identify increased anterograde Cab45G trafficking in obese humans with and without T2D, consistent with the heightened demand for granule biogenesis. However, humans with T2D demonstrate decreased Golgi Cab45G localization and increased granule Cab45G localization compared to those without T2D. Our study provides the first insight into Cab45G function in specialized secretory cells and opens avenues of investigation into mechanisms associated with β-cell compensation and failure.

INTRODUCTION

Pancreatic β-cells regulate insulin and insulin secretory granule biosynthesis to match the external requirement for blood glucose control. The precursor, proinsulin, is generated in the endoplasmic reticulum (ER) and advances to the *trans*-Golgi network (TGN), where it undergoes sorting into immature secretory granules before proteolytic conversion to insulin and development into mature secretory granules.[1,2] Secretion-competence declines as insulin granules age,[3] therefore, increased exocytotic output imposes pressure on the secretory pathway to replenish a population of young-mature granules through nascent biogenesis. This is handled well by healthy β-cells during acute bouts of hyperglycemia.[4] Capacity is assessed during chronic hyperglycemia, where secretory failure may arise from the insufficient production of insulin-rich mature granules and the premature release of proinsulin-rich immature granules.[5] The discovery of factors that drive insulin granule production is therefore central to understanding type 2 diabetes (T2D) pathogenesis.

There has been remarkable progress in understanding insulin transcription, translation, folding in the ER, and ER to Golgi transport.[6] It is known that defects in these processes contribute to diabetes susceptibility.[6] The mechanisms that control proinsulin trafficking through the Golgi apparatus and into immature granules, however, are less clear.[7] A soluble Golgi-localized Ca^{2+}-binding protein, Cab45G (45 kDa calcium-binding protein, *SDF4*), is the principal component of a secretory cargo sorting pathway in HeLa cells[8] which is dependent on the control of Cab45G oligomerization.[9,10] Ca^{2+}-binding promotes Cab45G assembly into large molecular weight oligomers for retention within the Golgi,[9] and subsequent phosphorylation reduces its oligomeric size to favor Cab45G-cargo trafficking into budding vesicles.[10] Our hypothesis is that Cab45G maintains the storage pool of insulin by facilitating protein delivery into immature granules. To date, this pathway has been characterized in HeLa cells with respect to constitutive secretion, but involvement in the regulated secretory pathway is unknown. All established components of this pathway are expressed in β-cells with some implicated in secretory pathway

function,[11,12] and interactions between Cab45G and proinsulin have been documented.[13]

Cab45G is a product of the *SDF4* gene. Other documented *SDF4* products are Cab45S and Cab45C present in the ER and cytosol, respectively.[14] Where possible, Cab45 isoforms have been specified in this article. Cab45S has not been studied in β-cells but it has been reported that Cab45C controls insulin granule exocytosis in primary rat β-cells through binding Munc18b.[15] *SDF4* mRNA levels increase in islets from obese non-diabetic *ob/ob* mice,[16] and total Cab45 protein abundance decreases in islets from humans with T2D compared to non-diabetic humans controlled for body mass index (BMI) ($log_2FC = -0.208$, adj. $p = 0.038$, $t = -2.66$).[17]

In this article, we extend the study of Cab45G to specialized secretory cells by providing an initial characterization in the context of disease phenotypes found in humans. We find that Cab45G is not required for granule biogenesis under normal physiological conditions, but it facilitates increased biogenesis which is an essential aspect of the β-cell response to metabolic stress. Cab45G overexpression upregulates granule production in a Ca^{2+}-independent process, demonstrated by a Cab45G mutant that cannot bind Ca^{2+} but produces more granules than Ca^{2+}-bound Cab45G. Despite superior production, the mutant also occupies a lower proportion of resultant granules compared to Ca^{2+}-bound Cab45G. In humans, Cab45G is present in both perinuclear Golgi and peripheral vesicular/granular compartments, with localization to the latter increasing in obesity and T2D. Humans with T2D, however, show increased granule-localized and decreased perinuclear Cab45G compared to humans without diabetes, who contain more Cab45G in non-insulin-containing vesicles and ample amounts of perinuclear Cab45G. Aberrant Cab45G localization could limit nascent granule biogenesis and interfere with granule function in β-cells from humans with T2D, warranting further investigation.

RESULTS

SDF4 expression is heterogeneous across tissues in mice

At this point in time, mammalian Cab45/*SDF4* expression remains poorly characterized. We applied complementary probes to *SDF4* mRNA in adult mouse tissue which revealed mostly ubiquitous, but heterogeneous, expression (Figures S1A–S1D), consistent with evidence in humans.[18] *SDF4* mRNA was prominent in endocrine, exocrine, and neural tissues and particularly enriched within sub-specialized regions of adrenal and pituitary glands. This is indicated by grainy silver staining concentrated in the adrenal medulla and anterior/intermediate lobes of the pituitary (Figures S1E–S1L), correlating with the presence of cell types that participate in the regulated secretion of key hormones that are critical for systemic function.[19–21]

Cab45G is expressed in the pancreatic islets of langerhans

Minimal *SDF4* mRNA detection across the pancreas (Figures S1C and S1D) could be due to the high abundance of pancreatic RNAses, leading us to immunostain fixed pancreas sections with an antibody raised against the full-length Cab45G protein[8] alongside insulin and glucagon (Figure 1A). Cab45G was mostly absent from exocrine tissue (Figure 1B) but present in β-cells from mice and humans, and α-cells from mice but not humans (Figure 1A), demonstrating that Cab45G is not ubiquitously expressed. Cab45G was visualized as "ribbon" structures adjacent to the nucleus, typical of Golgi staining, and as punctate structures spread throughout the cell-periphery of islet cells, characteristic of vesicular staining (Figure 1A). There was considerable variability between humans: β-cells from individual #1 contained mostly perinuclear Cab45G while #2 and #3 contained more punctate Cab45G, and individual #3 contained many insulin/glucagon-negative islet cells that were Cab45G-positive (Figures 1C and Table S1).

Peripheral Cab45G localization increases with the degree of human obesity

To further investigate determinants of Cab45G variability between humans, we immunostained Cab45G and total-insulin (insulin) in pancreas sections from non-diabetic (ND) and type 2 diabetic (T2D) human donors (Table S1). To investigate global changes in distribution, we used low-magnification images of whole-islets where insulin granules cannot be differentiated from one another, and calculated Manders' coefficients between Cab45G and insulin (Figures 2A and 2B). The Manders' coefficient of colocalization controls for variation in insulin abundance that could be present between humans, using insulin as a proxy that captures the non-nuclear β-cell area when processed using a low threshold. We found a positive correlation between increasing Manders' coefficient and BMI (Figure 2B, $r^2 = 0.29$, $p = 0.04$), independent of diabetic status. This demonstrates increased Cab45G localization in vesicular/ISG compartments during β-cell compensation, which continues into failure, consistent with the ongoing demand for insulin production.

Localization of Cab45G to insulin secretory granules increases in type 2 diabetes

To investigate the precise locality of vesicular/granular Cab45G during disease, we calculated Pearson's and Manders' coefficients between Cab45G and insulin in high-magnification images of β-cells within islets (Figure 2C). Here, we processed images using a high threshold to distinguish between punctate vesicular structures. Humans with T2D contained a higher proportion of insulin granules colocalizing with Cab45G compared to ND humans, where peripheral Cab45G occupied more non-insulin-containing vesicles (Figures 2D–2F).

Perinuclear Cab45G is lost from a subset of β-cells in humans with type 2 diabetes

We then quantified the number of β-cells that contained perinuclear Cab45G staining in ND and T2D humans (Figures 2G and 2H). For this analysis, the vesicular/granular Cab45G signal was digitally suppressed and we manually counted the number of nuclei encapsulated by insulin staining, and then the number of nuclei that had adjacent Cab45G staining. Humans with T2D contained a lower percentage of β-cells with perinuclear Cab45G (Figure 2H) in line with reduced *SDF4* mRNA levels in

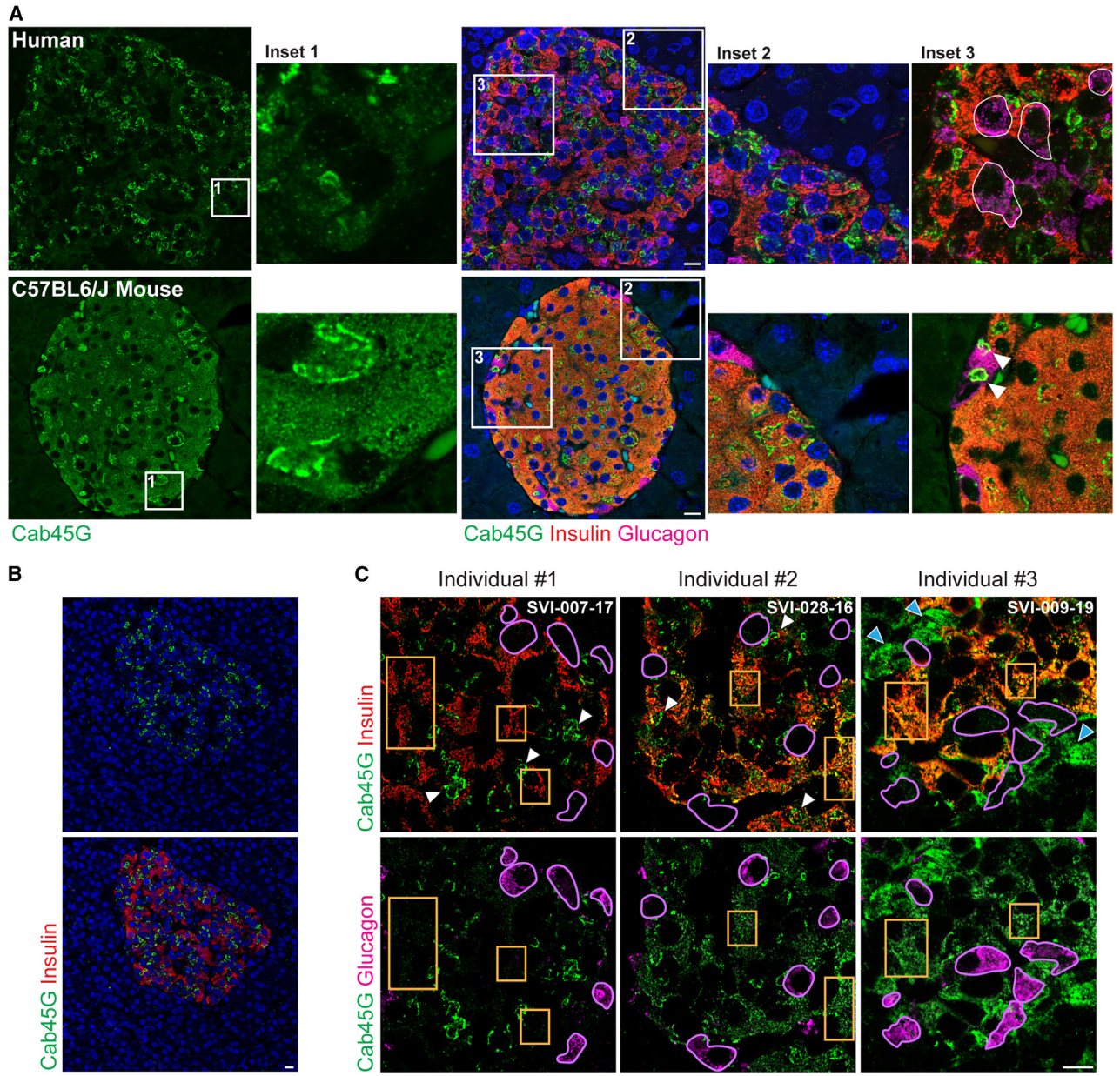

Figure 1. Pancreatic Cab45G expression and localization in mice and humans

Immunofluorescent staining of Cab45G, insulin and glucagon with DAPI in formalin-fixed 5 μm thick pancreas sections.

(A) Representative sections from humans and mice showing expression of Cab45G in pancreatic islets in perinuclear and vesicular/granular compartments (inset 1), absence of expression in adjacent exocrine tissue (inset 2), and respective presence/absence of Cab45G (white arrows) in mouse/human α-cells (white outlines) (inset 3), scale bar = 10 μm.

(B) Zoomed-out human islet showing absence of Cab45G expression in exocrine cells, scale bar = 10 μm.

(C) Variability in β-cell Cab45G subcellular localization in three separate humans (Table S1). Orange boxes refer to the peripheral regions of β-cells, irregular purple outlines encapsulate α-cells (reconfirming the absence of Cab45G), white arrows point to perinuclear Golgi-localized Cab45G, blue arrows point to Cab45G-positive cells not positive for either insulin or glucagon, scale bar = 10 μm.

islets from T2D donors,[17] suggesting that potential avenues of Golgi replenishment are impaired in the presence of increased trafficking. Our findings so far establish key associations between Cab45G locality and β-cell function, where Cab45G trafficking appears aberrant in humans with T2D.

Perinuclear Cab45G is localized in the cis-Golgi

To investigate β-cell Cab45G behavior we turned to the rat insulinoma cell-line, INS1. Immunostaining showed predominant localization of endogenous Cab45G to the *cis*-Golgi of INS1 cells (Figures 3A and 3B), but not the TGN as in HeLa cells[8] nor the

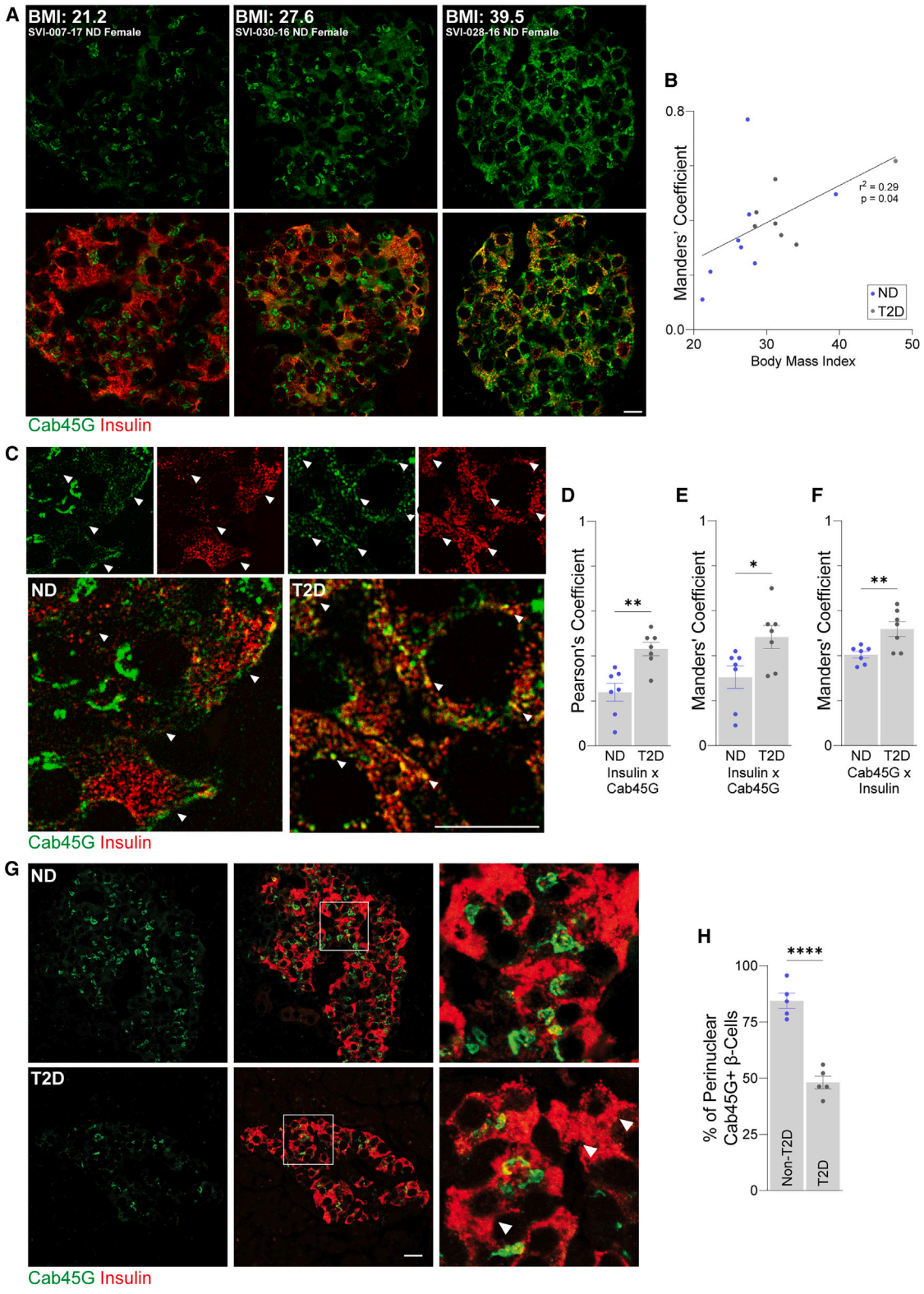

(legend on next page)

cell-periphery as in primary β-cells (Figure 1). Co-staining with insulin or a proinsulin-specific antibody revealed partial overlap between Cab45G and perinuclear proinsulin (Figure 3A), consistent with documented interactions,[13] indicating a potential relationship.

Cis-Golgi Cab45G localization is dependent on calcium

In HeLa cells, Ca^{2+}-binding is required for Cab45G oligomerization which is its TGN retention strategy.[8,9] To determine whether the *cis*-Golgi localization of β-cell Cab45G is dependent on Ca^{2+}, we examined its sensitivity to ionomycin, a Ca^{2+} ionophore. INS1 cells were Ca^{2+}-depleted for 20 min using ionomycin and EGTA in a Ca^{2+}-free medium. Perinuclear Cab45G dispersed and redistributed away from GM130-and TGN38-positive compartments into non-insulin-containing vesicles (Figures 3C and 3D). Unlike HeLa cells where Cab45G was absent from the cell after 5 min of Ca^{2+}-depletion,[8] INS1 cells retained Cab45G after 20 min of treatment.

Cab45G trafficks anterograde through the trans-Golgi network

Although endogenous Cab45G is undetectable outside the INS1 *cis*-Golgi (Figures 3A and 3B), primary β-cells contain abundant Cab45G spread throughout vesicular/granular compartments (Figures 1 and 2). To examine the nature of anterograde trafficking, we employed the retention using selective hooks system in INS1 cells.[22] Wild-type Cab45G tagged with green fluorescent protein (WT-Cab45G-GFP) or a Cab45G mutant unable to bind Ca^{2+} (6EQ-Cab45G-GFP)[9] were hooked in the ER using streptavidin (Figure 3H). A TGN-localized enzyme, Sialyltransferase, was tagged with red fluorescent protein (sialyltransferaseRFP)[23] and co-expressed to assess anterograde movement through the TGN.

Following biotin-mediated release, both variants trafficked anterograde through the TGN (Figure 3E). Due to reduced ER exit-rate 6EQ-Cab45G-GFP took 10 min/1.7 times longer than WT-Cab45G-GFP to reach the TGN (Figures 3E and 3F). Ca^{2+}-binding thus appears to influence Cab45G trafficking dynamics in the ER, potentially through conformational change. Rapid transit past the *cis*-Golgi suggests that the endogenous pool of Cab45G is highly dynamic, where overexpression beyond its holding capacity causes Cab45G to traffic distal. Both variants exited the TGN at the same rate indicating routing to the same class of vesicle (Figure 3G). Thus, while Ca^{2+}-binding is required for *cis*-Golgi Cab45G localization (Figures 3C and 3D), it does not prevent trafficking beyond this compartment.

INS1 Cab45G migrates as a doublet via gel electrophoresis

We generated CRISPR/Cas9-mediated Cab45KO INS1 cells to investigate Cab45G function in β-cells (Figure S2A). Using antibodies raised against full-length Cab45G we confirmed KO via immunofluorescence (Figure S2B) and observed the absence of a double-band above the 37 kDa marker on immunoblot (Figure S2C).

INS1 cells likely do not express Cab45C and Cab45S isoforms

Proteomics analysis showed complete loss of Cab45 peptides (Figure S2D). So far, we have been unable to validate the expression of other isoforms in INS1 cells due to antibody inaccessibility. Indeed, the known Cab45C and Cab45S isoforms have not been verified in rat[24] despite prior evidence of Cab45C expression in primary rat β-cells.[15] In humans, Cab45C is a 130-residue form of Cab45G containing identical amino acids 232–362, therefore, the insertion of a premature stop codon at residues 29–30 on Cab45G (Figure S2A) should not eliminate Cab45C expression from KOs. Moreover, in controls there were no identified peptides of the C-terminal sequence of Cab45S, which differs to Cab45G from residues 305 onward. These observations indicate that Cab45C and Cab45S are not expressed in INS1 cells.

Cab45KO INS1 cells are depleted of insulin secretory granules

During standard culture conditions in 11 mM glucose (11G), KOs had a 3-fold reduction in insulin granule abundance (Figures 4A and 4B). The insulin remaining in KOs was predominantly localized in the Golgi, likely in the form of proinsulin, compared to controls where insulin was abundant in both the Golgi and cell-periphery (Figures 4C and 4D). Accumulation here is consistent with evidence of a rate-limiting step in proinsulin trafficking in the Golgi observed in normal[25] and hyperglycemic[26] conditions, the latter being specified during TGN export.

Figure 2. Cab45G localization during β-cell compensation and failure in humans

Pancreas sections from non-diabetic (ND) and type 2 diabetic (T2D) human donors immunostained with Cab45G and insulin (Table S1).

(A and B) Pancreatic islets from three representative ND female donors depicting the relationship between increased Cab45G presence in the cell-periphery of islet cells and increasing body mass index (BMI), scale bar = 10 μm. (B) Simple linear regression model comparing BMI and Manders' overlap coefficient between Cab45G and insulin signals (M1), measured across whole-islets in at least three islets per donor and averaged (n = 15: 8 ND and 7 T2D). Here, at low magnification/resolution, insulin is a proxy for the cell-periphery.

(C–F) High magnification/resolution images of representative β-cells depicting the differential localization of vesicular/granular Cab45G (white arrows) in islets from ND and T2D human donors, scale bar = 5 μm. For colocalization analysis (D-F), calculations were performed on small groups of cells with perinuclear/Golgi-localized Cab45G and insulin signals excluded in at least three islets per donor (n = 7 per condition), presented as mean ± SEM. (D) Pearson's coefficient of correlation between vesicular/granular Cab45G and granular insulin, (E) Manders' overlap coefficients (M1 and M2) describing the fraction of granular insulin colocalizing with vesicular/granular Cab45G, (F) Manders' coefficient of correlation describing the fraction of vesicular/granular Cab45G colocalizing with granular insulin.

(G and H) Representative low magnification/resolution images of pancreatic islets from ND and T2D donors with white arrows pointing to the loss of Golgi-localized Cab45G from cells β-cells in T2D, scale bar = 10 μm. DAPI staining present and used for cell-counting but not shown. The vesicular/granular Cab45G signal was digitally suppressed for the manual quantification of Golgi-localized Cab45G. (H) Number of Golgi-localized Cab45G-positive cells expressed as a percentage of the total number of β-cells (n = 5 per condition), presented as mean ± SEM. Five islets per donor were quantified and averaged. β-cells (DAPI- and insulin-positive) and perinuclear Cab45G ribbon structures were manually counted (blinded) using FIJI (ImageJ) software. Comparisons made using unpaired t-test. (*, $p < 0.05$; **, $p < 0.01$; ****, $p < 0.0001$).

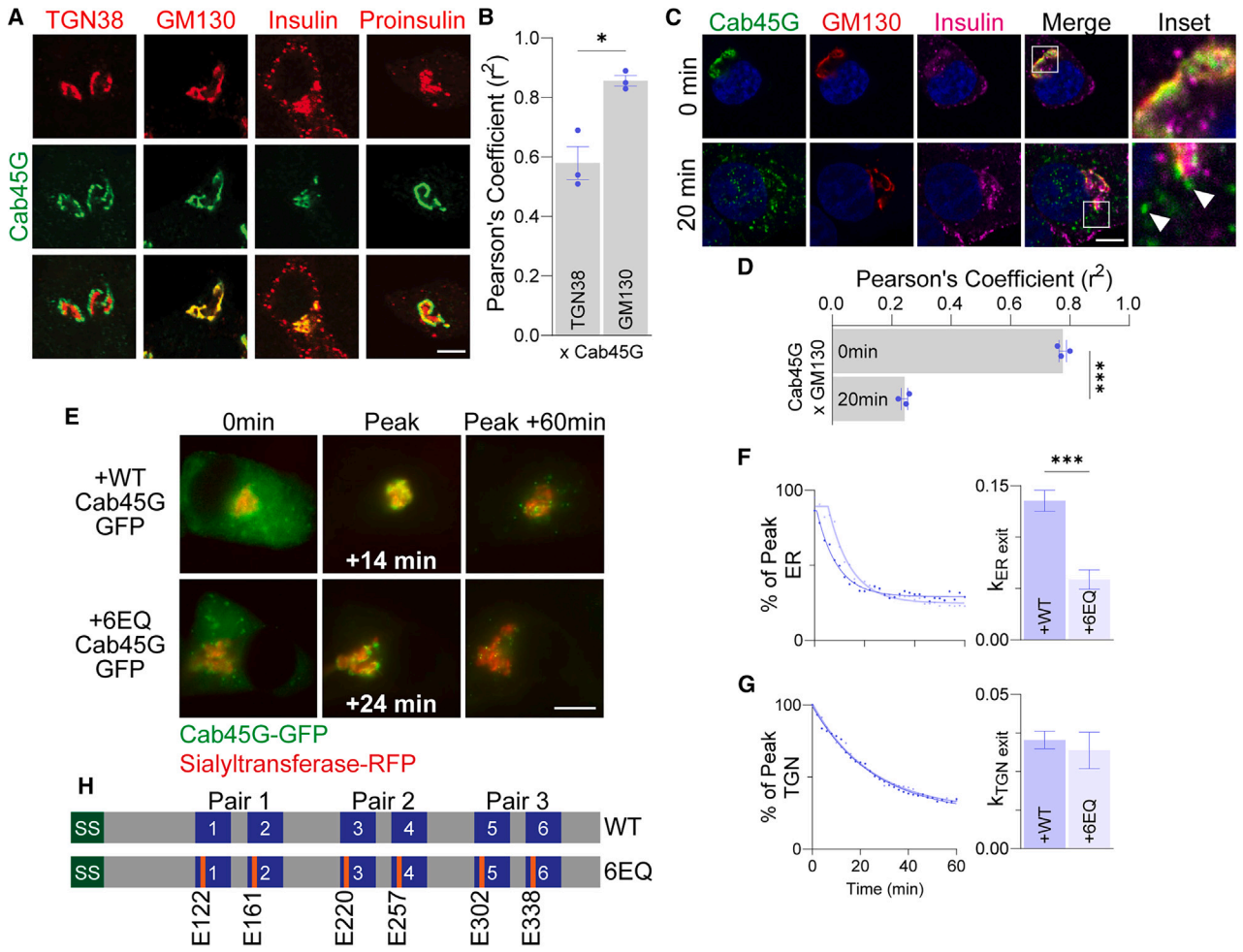

Figure 3. Ca^{2+}-dependency of the *cis*-Golgi Cab45G localization and visualization of anterograde trafficking in INS1 cells

(A) Immunofluorescent staining of Cab45G with either TGN38, GM130, insulin or proinsulin in INS1 cells (n = 3), scale bar = 5 μm.

(B) Pearson's coefficient of correlation between Cab45G and TGN38 versus Cab45G and GM130, presented as mean ± SEM.

(C and D) INS1 cells treated with ionomycin and EGTA in a Ca^{2+}-free medium for 20 min (n = 3). Cells were fixed and stained with antibodies targeting Cab45G, insulin, and GM130, scale bars = 5 μm. White arrows indicate post-Golgi Cab45G-positive vesicles. Manders' coefficient of colocalization was used to describe the fraction of cellular Cab45G localized in the *cis*-Golgi with GM130 (D), presented as mean ± SEM.

(E–G) Live visualization of WT- and 6EQ-Cab45G tagged with green fluorescent protein (GFP) trafficking from the ER through the TGN during the application of the retention using selective hooks (RUSH) protocol in INS1 cells, scale bar = 5 μm Cab45G-GFP variants were held in the ER using a streptavidin hook prior to release via biotin addition, and trafficking through the TGN was monitored with free co-expression of TGN-resident protein Sialyltransferase fused to red fluorescent protein (RFP). Labels indicate time to reach peak TGN-localization following release of Cab45G-GFP variants from the ER.

(F) Percentage of the peak ER-localized GFP signal intensity (left) and quantification of the rate of ER exit (right), and (G) Percentage of the peak TGN-localized GFP signal intensity (left) and quantification of the rate of TGN exit (right), presented as mean ± SEM.

(H) Schematic representation of WT- and 6EQ-Cab45G proteins displaying sites of point mutation (orange) to render the six Ca^{2+}-binding sites (blue) non-functional. Comparisons made using one-way ANOVA, paired, or unpaired t-test (**, $p < 0.01$; ***, $p < 0.001$; ****, $p < 0.0001$), with (F) and (G) using non-parametric testing.

Cab45G stimulates insulin secretory granule production

To assay the ability of Cab45G to generate insulin secretory granules, we transiently transfected plasmids containing hemagglutinin-tagged WT-Cab45G (WT-Cab45G-HA)[9] into KOs that contain a depleted insulin granule population (Figures 4A–4D) without any endogenous Cab45G (Figure S2B). We then measured the change in insulin distribution after 48 h. Overexpressed WT-Cab45G-HA trafficked anterograde into insulin granules and increased their abundance in the cell-periphery, reducing the proportion of insulin (proinsulin) located in the perinuclear region (Figures 4E and 4F).

Calcium-binding to Cab45G is not required for facilitated insulin secretory granule biogenesis

Ions drive conformational change in soluble proteins to facilitate sorting into, and retention within, developing granules.[27–29] We

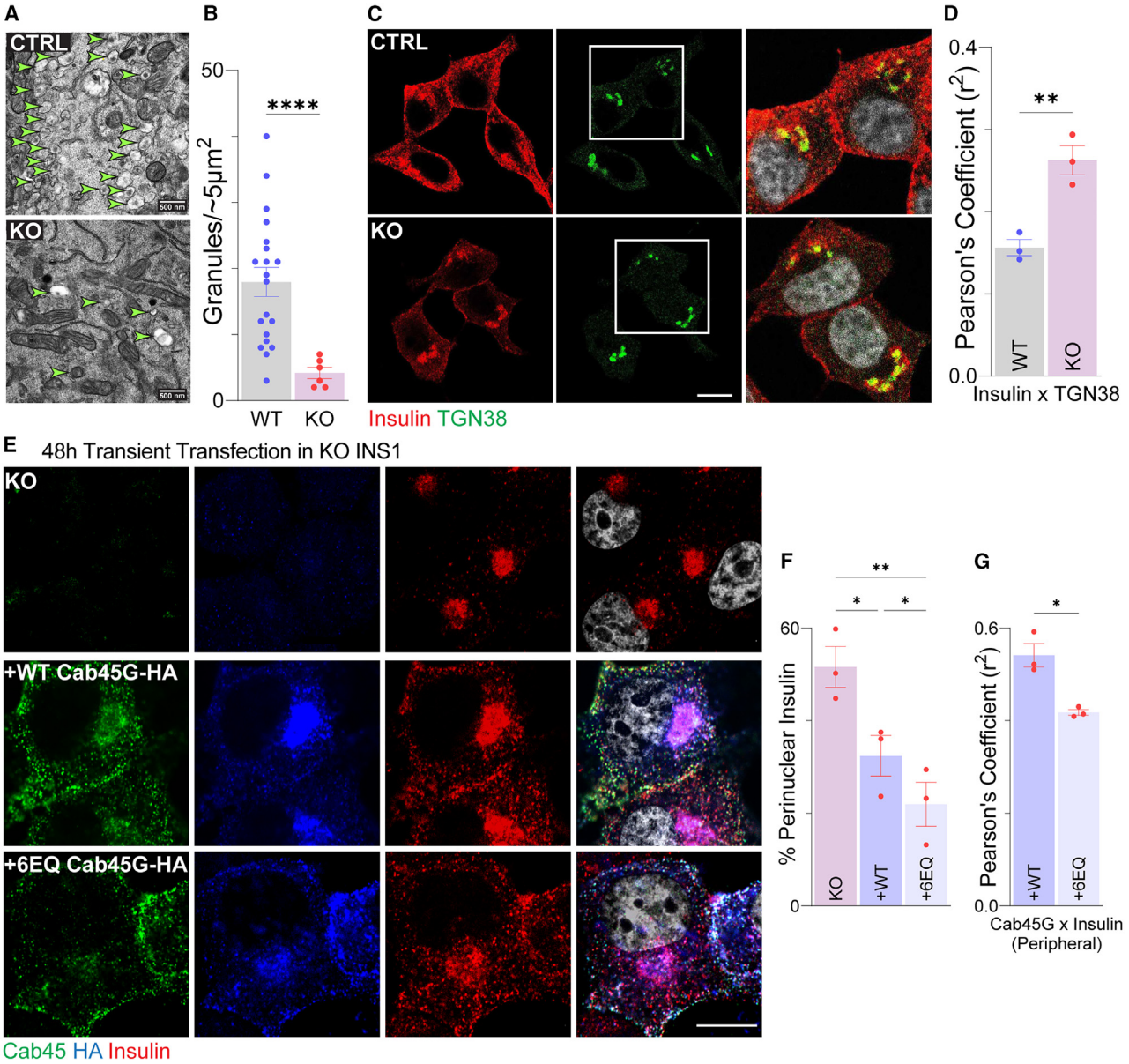

Figure 4. Insulin granule depletion in Cab45KO INS1 cells and influence of Ca^{2+}-binding to overexpressed Cab45G on granule rescue

(A and B) Electron microscopy of control (WT) and Cab45KO (KO) INS1 cells using immunogold labeling of insulin indicated by bright green arrows, scale bars = 500 nm. (B) Quantification of insulin granule abundance per 5 μm^2, with individual cells used as data points (WT: $n = 20$, KO: $n = 6$), presented as mean ± SEM. (C and D) Immunofluorescent staining for insulin and TGN38 ($n = 3$), scale bar = 10 μm. (D) Pearson's coefficient of correlation between insulin and TGN38 signal. (E–G) Immunofluorescent staining of Cab45G, HA, and insulin in KO INS1 cells cultured in standard conditions at 11 mM glucose re-expressing WT- or 6EQ-Cab45G-HA, scale bar = 10 μm. (F) Percentage of total cellular insulin residing in the perinuclear Golgi region quantified in at least 10 cells per replicate ($n = 3$), presented as mean ± SEM. (G) Pearson's coefficient of correlation between overlaid Cab45G/HA signal with the insulin signal, with perinuclear/Golgi-localized signals excluded, measured in at least 10 cells per replicate ($n = 3$) and presented as mean ± SEM. Comparisons made using one-way ANOVA or paired t-test (*, $p < 0.05$; **, $p < 0.01$), with (B) using non-parametric testing.

examined the role of Ca^{2+}-binding to Cab45G in insulin granule production using HA-tagged 6EQ-Cab45G (6EQ-Cab45G-HA).[9] Surprisingly, 6EQ-Cab45G-HA brought about superior rescue of peripheral insulin distribution compared to WT-Cab45G-HA (Figures 4E and 4F). Thus, while Ca^{2+}-bound Cab45G can facilitate a high degree of granule production, Ca^{2+}-free Cab45G performs better in this regard. This demonstrates that unlike HeLa cells,[9] β-cell Cab45G-dependent trafficking does not require Ca^{2+}-binding.

Calcium-binding increases the insulin secretory granule localization of Cab45G

Both WT- and 6EQ-Cab45G-HA variants were visually abundant throughout vesicular/granular compartments (Figure 4E),

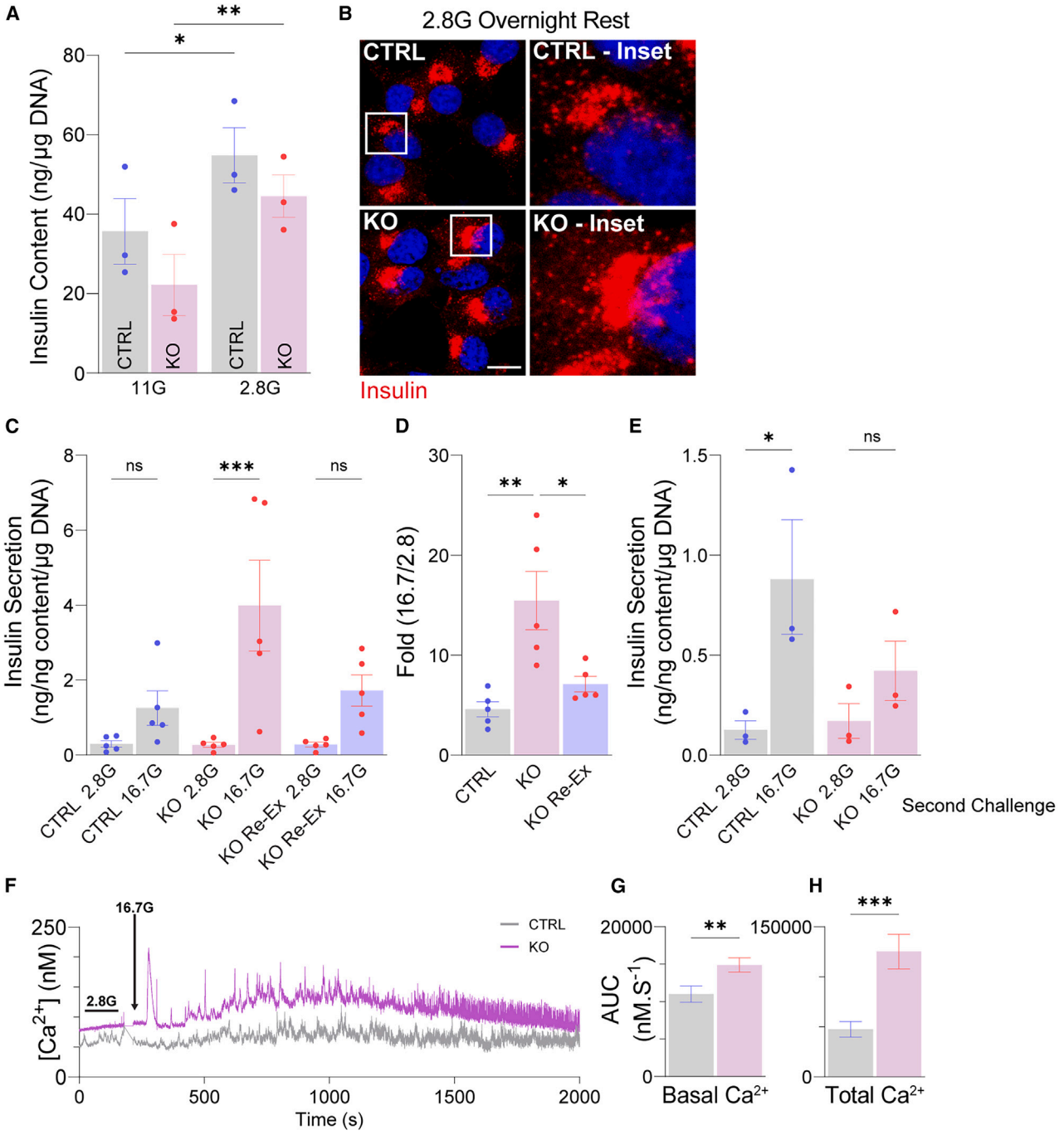

Figure 5. Dysregulated insulin secretion and Ca^{2+} homeostasis in Cab45KO INS1 cells

(A) Quantification of insulin content with DNA normalization during standard 11 mM (11G) and low 2.8 mM (2.8G) glucose RPMI-1640 culture overnight (n = 3), presented as mean ± SEM.

(B) Immunofluorescent staining of insulin in cells cultured at 2.8 mM glucose (n = 3), scale bar = 10 µm.

(C–E) Glucose-stimulated insulin secretion (GSIS) assays in control (WT) or Cab45KO (KO) INS1 cells with and without re-expressed WT-Cab45G tagged with hemagglutinin (HA) (Re-Ex). Cells were rested overnight in low 2.8 mM glucose RPMI-1640 prior to pre-basal in 2.8 mM glucose Krebs buffer, and then incubated for 1 h in either 2.8 mM (2.8G) or 16.7 mM (16.7G) glucose Krebs buffer. Secreted insulin was normalized to cellular insulin content and DNA (C) or expressed as the fold change from 2.8G to 16.7G (D) and presented as mean ± SEM. (E) GSIS in WT and KO cells with additional 16.7G challenge 30 min after the initial challenge. Secreted insulin from the second challenge was normalized to cellular insulin content and DNA, presented as mean ± SEM. (F-H) Cells loaded with Fura-2 a.m. dye were stimulated with 16.7G for 45 min following overnight rest at 2.8G (n = 3).

(legend continued on next page)

consistent with <48 h of ectopic expression and the 3–5 days half-life of insulin granules.[6] To examine the influence of Ca^{2+}-binding on Cab45G trafficking in post-Golgi compartments, we measured Pearson's coefficient between Cab45G-HA variants and insulin exclusively in the cell-periphery and found that 6EQ-Cab45G-HA colocalized less with insulin compared to WT-Cab45G-HA (Figure 4G). That is, Ca^{2+}-bound Cab45G had a greater propensity to colocalize with insulin granules in what may be an undesirable outcome considering phenotypic parallels with the pathological state of T2D (Figures 2C–2F). The combination of improved granule output with reduced granule colocalization suggests that Cab45G performs optimally without Ca^{2+}-binding. This is consistent with the tendency of Cab45G to form oligomers in the presence of Ca^{2+} that resist trafficking, which can be alleviated through phosphorylation to enhance mobility.[9,10]

Overnight rest at low glucose restores insulin content in Cab45KO INS1 cells

So far, our findings indicate that proinsulin trafficking is inhibited in the absence of Cab45G. However, limiting insulin secretion by overnight rest in RPMI-1640 containing 2.8 mM glucose (2.8G) raised KO insulin content (Figure 5A) and reinstated an abundance of peripheral insulin (Figure 5B). Thus, while Cab45G accelerates granule production, it is not required by the β-cell to traffic proinsulin and synthesize insulin granules. This suggests that insulin granules in KOs cultured at the moderately high concentration of 11G are lost to an alternative mechanism.

Insulin hypersecretion leads to degranulation in Cab45KO INS1 cells

Insulin granule abundance is dependent on rates of production, degradation, and exocytosis. To assess differences in exocytosis, we performed glucose-stimulated insulin secretion (GSIS) experiments at 16.7 mM glucose (16.7G) following the normalization of insulin content by overnight rest in 2.8G RPMI-1640.

Basal insulin secretion was unaffected in KOs, arguing against a proinsulin sorting by entry defect (Figure 5C). Stimulated secretion at 16.7G was 3-fold higher in KOs and this was rescued by WT-Cab45G-HA overexpression (Figures 5C and 5D). When KOs were exposed to a second glucose stimulus 30 min after the initial challenge, secretion became limited (Figure 5E). Using Fura-2 AM, we found that elevated cytosolic Ca^{2+} concentrations in KOs during glucose stimulation (Figures 5F and 5H) underlies hypersecretion, leading to degranulation in KOs, but increased basal Ca^{2+} concentrations (Figures 5F and 5G) did not translate to increased basal insulin release (Figure 5C). Notably, we also observed reduced levels of proinsulin secreted at both low glucose and during stimulation (Figure S3).

INS1 proteomic adaptations to chronic Cab45 loss

Proteomics analysis revealed that around 10% of quantified proteins were differentially expressed in KOs, with most downregulated (Figures S2E and S2F). This includes hallmark granule-resident proteins (Figure 6A) that reflect the depleted granule population in KOs cultured at 11G (Figures 5A and 5B).

Upregulation of ER-localized Ca^{2+} regulators *SRI* and *ITPR3*[30–32] and downregulation of the Golgi-localized Ca^{2+}-binding protein *NUCB2* (cleaved to form the secreted peptide Nesfatin-1[33,34]) (Figure 6A) provide indications of altered secretory pathway Ca^{2+}-handling in KOs. *ITPR3* also localizes to insulin granules[35] but was upregulated despite granule loss; thus, increased ER-localized *ITPR3* could be under-represented.

SRI and *ITPR3* facilitate ER Ca^{2+} exchange with the mitochondria which, with cytosolic Ca^{2+}, regulates mitochondrial metabolism.[30–32,36] Many components of the electron transport chain involved in oxidative phosphorylation were downregulated in KOs, with particular representation from complexes I and IV (Figures 6A–6C). Mitochondrial matrix proteins *GLS*, *GCLC* and *GCLM* involved in glutamate metabolism[37] were upregulated whereas *PC* involved in pyruvate metabolism[38] was downregulated in KOs (Figures 6A and 6B).

The affected proteome suggests chronic adaptation to redistributed organellar Ca^{2+}, initiated by Cab45G loss. These manifest predominantly in the mitochondria where changes resemble those caused by exposure to sustained hyperglycemia,[39] suggesting that Cab45G loss predisposes β-cells to metabolic dysfunction. This may be important considering the unique characteristics of Ca^{2+} handling by secretory organelles,[40] changes in Cab45 expression,[16,17] and Cab45G redistribution within the secretory pathway in obese and T2D humans (Figure 2).

DISCUSSION

The TGN serves as the initial branchpoint for secretory proteins on their journey to the extracellular space, where they are segregated into vesicular subpopulations that dictate their ultimate destination. In β-cells, over 99% of proinsulin is directed into immature insulin granules[41] - an impressive feat considering that preproinsulin can account for 50% of total protein synthesis.[6] Despite this precision, the search for a proinsulin sorting receptor has remained elusive. Preproinsulin is co-translationally regulated alongside approximately 50 granule-destined proteins, all undergoing synchronized trafficking.[42,43] However, the mechanisms governing this sorting process are still being uncovered.[7]

The "refined bulk flow" hypothesis suggests that proteins destined for the insulin granule are sorted based on their combined mass and their sensitivities to ion-induced aggregation.[44] Recent research showing that the H^+-induced liquid-liquid phase separation of chromogranin attracts proinsulin[45] supports this. Bulk flow into immature granules, though somewhat fairly non-selective, may represent the default pathway for soluble proteins, working alongside specific mechanisms that direct non-granule proteins elsewhere.[46] This aligns with the difficulty in identifying sorting receptors for granule-destined cargo but

(F) Representative traces of cytosolic Ca^{2+} concentration.
(G) Area under the curve (AUC) during a 3-min sample of 2.8G incubation prior to 16.7G stimulation or (H) the total time course of 2.8G basal plus 16.7G stimulation (WT: $n = 34$, KO: $n = 48$), presented as mean ± SEM. Comparisons made using one-way ANOVA, two-way ANOVA, or paired t-test (*, $p < 0.05$; **, $p < 0.01$; ***, $p < 0.001$), with (G) and (H) using non-parametric testing.

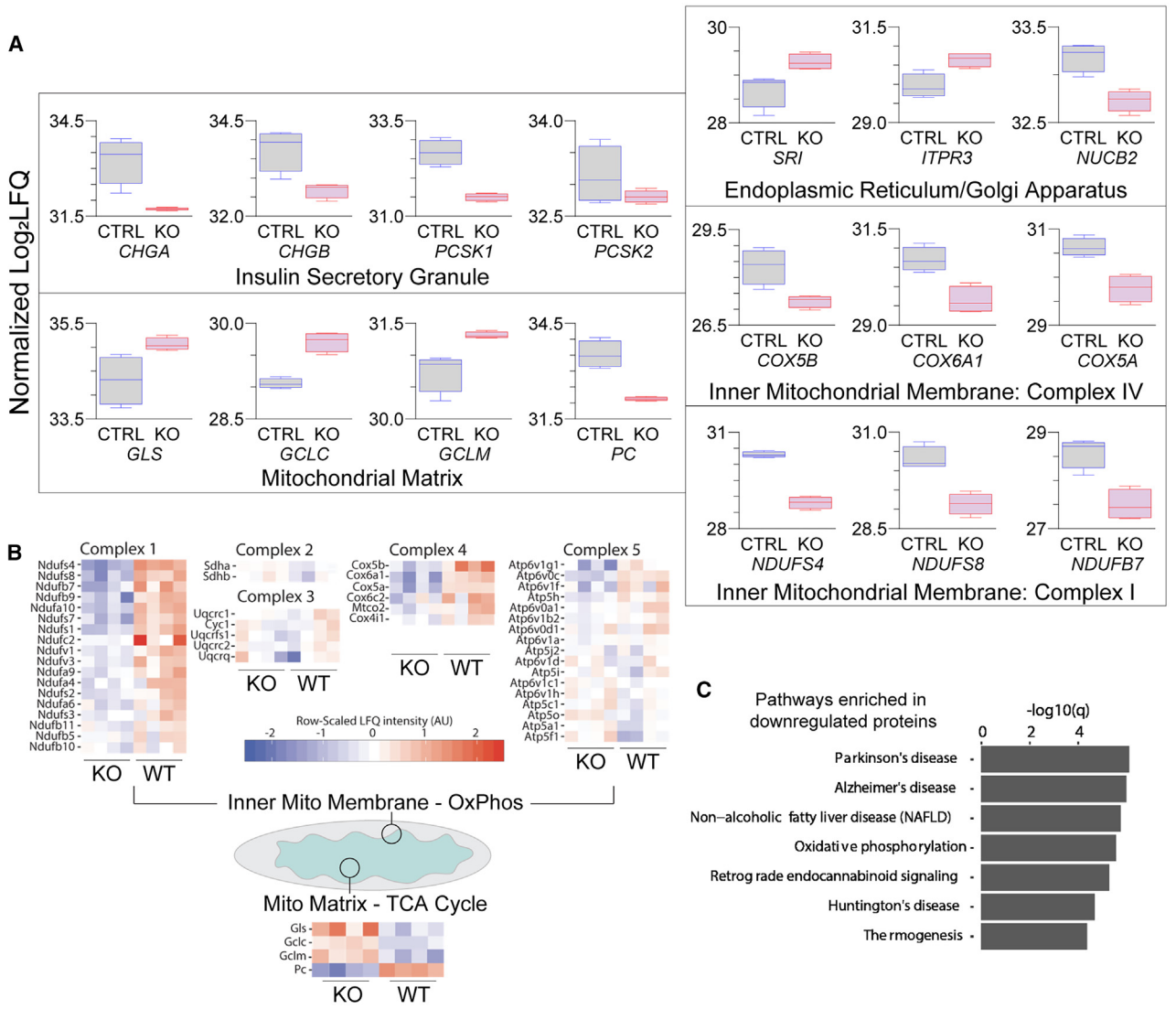

Figure 6. Proteomic adaptations to Cab45KO in INS1 cells

(A) Mass spectrometry-based quantitative proteomics of cells (n = 4) showing altered expression of select proteins (denoted by gene titles), presented as mean ±95% CI.

(B) Relative abundance of key mitochondrial proteins presented as scaled intensity.

(C) Gene set enrichment analysis of pathways with downregulated proteins in KOs.

fits with the role of soluble chaperones in facilitating protein trafficking.

The aim of our study was to examine if the Golgi-resident luminal protein, Cab45G, plays a role in the trafficking of proinsulin within β-cells. Cab45G has previously been recognized as a TGN-resident protein that is ubiquitously expressed.[8,47,48] We now identify its presence in mammalian islets but not in the exocrine pancreas, and within a dynamic, limited-capacity pool in the *cis*-Golgi of INS1 cells. Similar to TGN-Cab45G in HeLa cells,[8] it is concentrated in the *cis*-Golgi of β-cells by Ca^{2+}, but reasons for discrepant localization remain unclear. While insulin granules can be synthesized without Cab45G, its overexpression and movement through the TGN accelerates biogenesis as shown by the synchronized trafficking of Cab45G and proinsulin into a vast population of nascent granules. This tracks with evidence of Cab45G's interaction with proinsulin[13] and its function at the TGN,[8] suggesting that it acts as a non-essential chaperone that supports cargo trafficking.

We were surprised to observe increased granule production by the Ca^{2+}-free 6EQ-Cab45G mutant as it contradicts with previous evidence that Ca^{2+}-binding is required for client trafficking.[9] It is unclear why this occurs and is further complicated by the observation that both variants show efficient export from the TGN, yet 6EQ-Cab45G is present in fewer granules. One possible explanation could be that 6EQ-Cab45G dissociates from its bound cargo more easily than WT-Cab45G, resulting

in its release into non-insulin-containing vesicles from the TGN. Another possibility is that 6EQ-Cab45G and its bound cargo disperse more freely across the TGN, leading to the formation of more granules. Consistent with theories of default targeting into the immature granule,[46] 6EQ-Cab45HA enters these compartments as efficiently as WT-Cab45G but may be sorted for exit[44] more effectively.

The authors who postulated this theory overexpressed a truncated form of Cab45G in INS1 cells, demonstrating that when the 53 C-terminal residues are removed, Cab45G avoids the regulated secretory pathway and associates with membranes for targeting into constitutive vesicles.[46] The unstructured C-terminus of Cab45G[49] may therefore contain crucial information necessary for interaction with granule-destined cargo, independent of Ca^{2+}-binding. Moreover, it is known that Ca^{2+} supports aspects of regulated secretory cargo trafficking,[50] and our current study shows that global Ca^{2+} depletion using ionomycin and EGTA redirects Cab45G into non-insulin-containing vesicles. Based on the evidence, it seems possible that Ca^{2+}-bound granule-destined cargo directs Cab45G into the regulated secretory pathway through its C-terminus, and in turn, Cab45G enhances the bulk flow of cargo trafficking. This scenario is comparable to a cab driver (Cab45G) receiving instruction from their passengers (cargo). In theory, this mechanism could allow for compatibility with various cargo types found within the diverse set of mammalian secretory cells where Cab45G/*SDF4* is expressed.

The secretory pathway is endowed with luminal proteins that bind and quench Ca^{2+},[50] transforming this compartment into a complex system that buffers cytosolic Ca^{2+}.[51] Cab45 plays a significant role in this process, evidenced in HeLa cells where acute depletion of Cab45 reduces free Ca^{2+} levels in the TGN by more than half.[8] The redistribution of Ca^{2+} to other proteins with varying affinities and capacities for Ca^{2+} could explain the change, impacting the dynamics of cytosolic Ca^{2+} buffering within the secretory pathway and potentially leading to long-term changes in protein expression. In the present study, granule depletion in KOs occurs as a consequence of hypersecretion, resulting from cytosolic Ca^{2+} dysregulation. Proteomics analysis suggests that KOs have adapted to a modified Ca^{2+} environment throughout the secretory pathway and mitochondria. Several factors could trigger this, either directly via the loss of a major Ca^{2+}-quenching protein from the secretory pathway, or indirectly by disturbing the trafficking of Ca^{2+} transporters. Notably, we do not see any indication of ER/Golgi stress when Cab45 is depleted. Upstream responses in the ER are usually observed when insulin demand increases[52]; therefore, in our hypersecreting model, the absence of ER/Golgi stress is consistent with insufficient granule replenishment. On the other hand, increased Cab45G load through the secretory pathway occurs during β-cell compensation and failure and could contribute to the stress-response seen in diabetes.[53]

Indeed, increased insulin production during β-cell compensation leads to a robust Cab45 response at the biosynthetic level, as shown by increased *SDF4* mRNA in islets from *ob/ob* mice.[16] Overexpressing Cab45G beyond the *cis*-Golgi's holding-capacity can achieve anterograde trafficking, which increases with metabolic stress in humans and stimulates insulin granule biogenesis in INS1 cells. This mechanism persists in failing human β-cells despite a reduction in total Cab45 protein compared to BMI-matched non-diabetic humans.[17] In this case, Cab45G occupies a larger proportion of insulin granules and shows reduced perinuclear localization compared to non-diabetic humans. In INS1 cells, overexpressed Ca^{2+}-bound WT-Cab45G occupies a larger proportion of granules compared to Ca^{2+}-free 6EQ-Cab45G, aligning with Cab45G's tendency to form oligomers and aggregate in a Ca^{2+}-dependent manner[9] which favors retention inside the granule.[50] Therefore, when Cab45G biosynthesis increases, mechanisms that counteract Ca^{2+}-binding effects, such as phosphorylation at particular sites,[10] may be crucial for alleviating the diabetic phenotype. On the contrary, missense mutations could predispose to diabetes, indicated by an asparagine conversion to serine at residue 74 (rs11716727) that introduces a potential phosphorylation site and nearly doubles the likelihood of T2D in humans.[54]

In humans, Cab45G-associated dysfunction could manifest in two main ways. First, the absence of Cab45G from the Golgi in about 50% of failing β-cells may hinder β-cell compensation. While proinsulin acceleration is not required under normal physiological circumstances with excess insulin supply, it becomes crucial when increasing supply to meet elevated demand. During β-cell compensation, a progressive loss of Golgi-Cab45G could cause bottlenecks in proinsulin trafficking, limiting nascent biogenesis and contributing to diabetes.[5] Second, the presence of Cab45G within secretory granules might interfere with granule function. Although we have not studied the effects of excess granule-localized Cab45G, its aberrant localization in humans with T2D suggests that Cab45G needs to exit the maturing granule after performing its chaperon role. Key questions remain about why Cab45G becomes mislocalized in T2D and how this affects β-cell function.

Our findings, in conjunction with existing literature, suggest that during β-cell compensation, Cab45G is upregulated to sustain insulin secretory granule production. However, mechanisms that counteract the effects of Ca^{2+}-binding prior to Cab45G entering the immature granule favors its exit from the maturing granule, maintaining granule function (Figure 7). While facilitated insulin granule production is largely unaffected by Ca^{2+}-binding, this binding increases the propensity for Cab45G retention within granules. Predisposition toward β-cell failure may therefore be triggered by events in the Golgi, influenced by genetic factors regulating Cab45G behavior. Individuals with T2D might face a "double-whammy" due to Cab45G mislocalization: the loss of Golgi Cab45G limits nascent granule supply during chronic insulin demand, and granule-localized Cab45G disrupts granule function.

Limitations of the study

The limitations of this study are as follows. 1: The antibody raised against full-length Cab45G has not yet been validated against other isoforms. Although we show no evidence of Cab45C and Cab45S expression in INS1 cells, their presence in human and mouse islets cannot be ruled out – though we believe it is unlikely. 2: The hypersecretory behavior of Cab45KO INS1 cells could be masking a direct effect of Cab45G deletion on granule

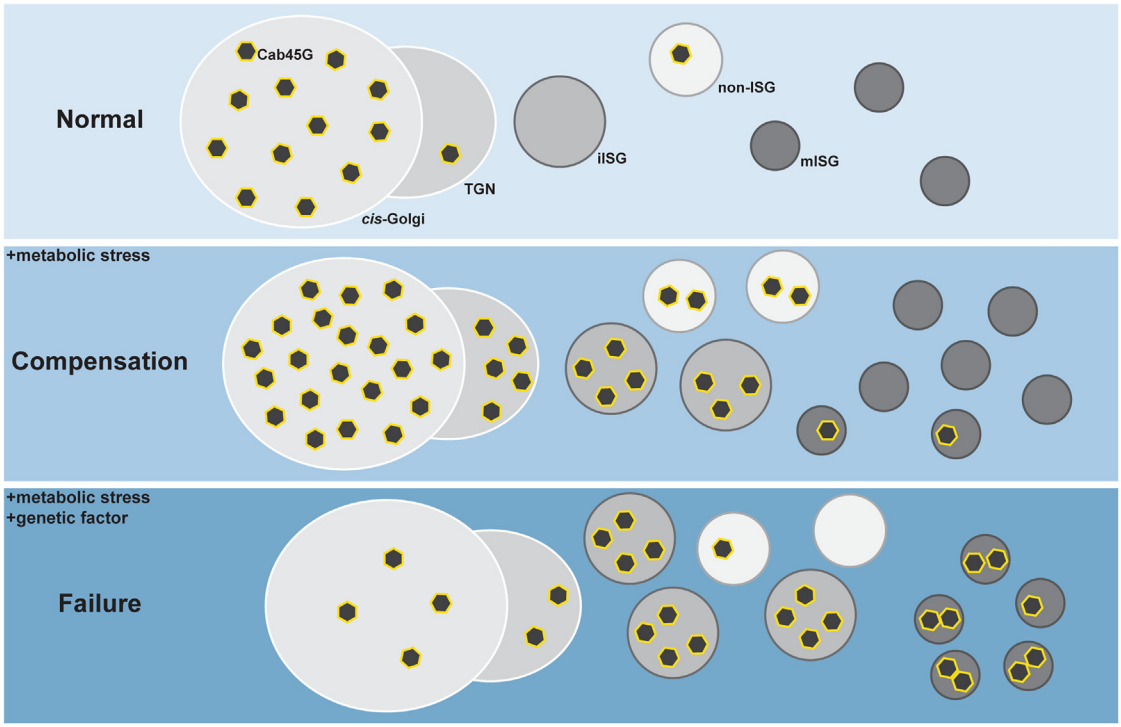

Figure 7. Current working model of Cab45G localization through stages of β-cell function

Key: ISG - insulin secretory granule, iISG - immature ISG, mISG - mature ISG, TGN - *trans*-Golgi network. During normal conditions (top), proinsulin trafficks through the TGN and into immature insulin secretory granules via bulk-flow. Since supply is in excess to demand it does so without the need for Cab45G-dependent acceleration; although this may be present to some extent, Cab45G predominantly resides in the *cis*-Golgi. Metabolic stress imposes pressure to synthesize and secrete insulin, and compensating β-cells (middle) respond by upregulating *SDF4* mRNA production which increases Cab45G biosynthesis beyond the holding-capacity of the *cis*-Golgi. This pushes Cab45G out from this compartment to accelerate bulk-flow trafficking and drive granule production. Cab45G may then exit the maturing granule into non-insulin secretory granules. Progression into β-cell failure (bottom) is associated with an aberrant pattern of Cab45G trafficking. While anterograde Cab45G trafficking is maintained, its abundance in the perinuclear area is reduced and it accumulates in the mature insulin secretory granule.

abundance. In this study we do not investigate proinsulin trafficking directly, which can be addressed in future studies using methods such as RUSH and pulse chasing. 3: our study relies on a male immortalized cell-line and *in vitro* experimentation. An *in vivo* rodent model containing both male and female subjects would be most ideal, where factors such as clonal heterogeneity[55–58] and sex, that could contribute to secretory variability are eliminated, and where animals can be subjected to diet-induced metabolic stress. 4: Chronic cellular adaptation to Cab45G loss may not be physiologically relevant since we do not see evidence for Cab45G absence in humans with T2D. Instead, transient silencing using siRNA may be more suited to this investigation where acute effects on proinsulin trafficking can be observed. These limitations were learnt during this initial investigation into Cab45G function in pancreatic β-cells and will be considered to optimize future work.

RESOURCE AVAILABILITY

Lead contact

Requests for further information and resources should be directed to and will be fulfilled by the lead contact, Melkam A Kebede (melkam.kebede@sydney.edu.au).

Materials availability

All unique/stable reagents, including the Cab45KO INS1 cell line and oligonucleotides, generated in this study are available from the lead contact with a completed materials transfer agreement.

Data and code availability

- **Data:** Proteomics data have been deposited as a ProteomeXchange dataset on the PRIDE database as PXD052042 and are publicly available as of the date of publication. All other data reported in this article will be shared by the lead contact upon request.
- **Code:** This article does not report original code.
- **Additional items:** Any additional information required to reanalyze the data reported in this article is available from the lead contact upon request.

ACKNOWLEDGMENTS

We would like to thank the following individuals for their contributions to this ongoing project: Andy Gao, Nicholas Norris, Louise Cottle, Victor Shahen, Cameron Cos, Essi Havula, Kiran Hasygar, Nabil G. Seidah, and David E. James. We would also like to thank the core facilities at the Charles Perkins Center at the University of Sydney. This study was made possible with access to the Sydney Mass Spectrometry and Sydney Microscopy and Microanalysis facilities. We thank the organ donors and their families for their generosity. We also thank the members of St Vincent's Institute in the islet isolation program and Donatelife for providing research consent and provision of human pancreata.

Funding: St Vincent's Institute receives support from the Operational Infrastructure Support Scheme of the Government of Victoria. This work was supported by National Health and Medical Research Council (NHMRC) project grant GNT1139828 (to M.A.K.) and by NIH grant R01 GM121481 (M.A.). M.G. was supported by the University of Sydney Postgraduate Award (UPA).

AUTHOR CONTRIBUTIONS

M.G., B.Y., and M.A.K. conceptualized this study. M.G. wrote this article with significant contributions from B.Y. and M.A.K. and minor contributions from M.T. and K.S. M.A., C.S.A, J.v.B., P.T., and D.E.J. provided consultation and direction. J.v.B. and C.S.A. provided critical reagents including plasmids, antibodies, and cell-lines. N.G.S. performed *in situ* hybridization experiments in mice. T.L. and H.T. prepared human pancreas sections. C.Y., M.G., and B.Y. conducted immunostaining in pancreas sections. B.Y. conducted subcellular fractionation of INS1 cells. B.Y. and A.W. conducted immunostaining of INS1 cells. M.T. and M.G. conducted ionomycin experiments in INS1 cells. D.M. and C.S.A. conducted RUSH experiments in INS1 cells. B.Y. conducted electron microscopy of INS1 cells. A.W. and M.G. measured insulin content and distribution in INS1 cells. B.Y., A.W., and Y.A. conducted insulin secretion experiments in INS1 cells. J.T. and P.T. conducted Fura-2 a.m. experiments in INS1 cells. M.G., S.N., E.J.N., M.T., and M.L. contributed to proteomics analysis of INS1 cells. M.T. and M.G. conducted overexpression and localization experiments in INS1 cells. J.C-O. and M.A. conducted informative experiments in INS1 cells that were not presented here. A.G.v.d.K. and K.S. provided general experimental assistance.

DECLARATION OF INTERESTS

M.A.K is a consulting editor for iScience. The authors declare no competing interests.

STAR★METHODS

Detailed methods are provided in the online version of this paper and include the following:

- KEY RESOURCES TABLE
- EXPERIMENTAL MODEL AND STUDY PARTICIPANT DETAILS
  - Human pancreas tissue
  - Rat insulinoma INS1 cell lines
  - Cab45KO INS1 cells
- METHOD DETAILS
  - *In situ* hybridization
  - Pancreas immunofluorescence staining
  - INS1 immunofluorescence staining
  - Transient DNA transfection
  - Cell harvest and immunoblotting
  - Retention using selective hooks (RUSH)
  - Transmission electron microscopy
  - Mass spectrometry-based proteomics
  - Glucose-stimulated insulin secretion (GSIS)
  - Ca^{2+} depletion in INS1 cells
  - Ca^{2+} imaging with Fura-2 a.m
- QUANTIFICATION AND STATISTICAL ANALYSIS

SUPPLEMENTAL INFORMATION

Supplemental information can be found online at https://doi.org/10.1016/j.isci.2024.111719.

Received: September 8, 2024
Revised: October 29, 2024
Accepted: December 28, 2024
Published: December 30, 2024

REFERENCES

1. Orci, L., Halban, P., Amherdt, M., Ravazzola, M., Vassalli, J.D., and Perrelet, A. (1984). Nonconverted, amino acid analog-modified proinsulin stays in a Golgi-derived clathrin-coated membrane compartment. J. Cell Biol. *99*, 2187–2192.
2. Smeekens, S.P., Montag, A.G., Thomas, G., Albiges-Rizo, C., Carroll, R., Benig, M., Phillips, L.A., Martin, S., Ohagi, S., and Gardner, P. (1992). Proinsulin processing by the subtilisin-related proprotein convertases furin, PC2, and PC3. Proc. Natl. Acad. Sci. USA *89*, 8822–8826.
3. Yau, B., Hocking, S., Andrikopoulos, S., and Kebede, M.A. (2021). Targeting the insulin granule for modulation of insulin exocytosis. Biochem. Pharmacol. *194*, 114821.
4. Yau, B., Hays, L., Liang, C., Laybutt, D.R., Thomas, H.E., Gunton, J.E., Williams, L., Hawthorne, W.J., Thorn, P., Rhodes, C.J., et al. (2020). A fluorescent timer reporter enables sorting of insulin secretory granules by age. J. Biol. Chem. *295*, 8901–8911.
5. Alarcon, C., Boland, B.B., Uchizono, Y., Moore, P.C., Peterson, B., Rajan, S., Rhodes, O.S., Noske, A.B., Haataja, L., Arvan, P., et al. (2016). Pancreatic β-Cell Adaptive Plasticity in Obesity Increases Insulin Production but Adversely Affects Secretory Function. Diabetes *65*, 438–450.
6. Rohli, K.E., Boyer, C.K., Blom, S.E., and Stephens, S.B. (2022). Nutrient Regulation of Pancreatic Islet β-Cell Secretory Capacity and Insulin Production. Biomolecules *12*, 335. https://doi.org/10.3390/biom12020335.
7. Campelo, F., Tian, M., and von Blume, J. (2023). Rediscovering the intricacies of secretory granule biogenesis. Curr. Opin. Cell Biol. *85*, 102231.
8. von Blume, J., Alleaume, A.-M., Kienzle, C., Carreras-Sureda, A., Valverde, M., and Malhotra, V. (2012). Cab45 is required for Ca(2+)-dependent secretory cargo sorting at the trans-Golgi network. J. Cell Biol. *199*, 1057–1066.
9. Crevenna, A.H., Blank, B., Maiser, A., Emin, D., Prescher, J., Beck, G., Kienzle, C., Bartnik, K., Habermann, B., Pakdel, M., et al. (2016). Secretory cargo sorting by Ca2+-dependent Cab45 oligomerization at the trans-Golgi network. J. Cell Biol. *213*, 305–314.
10. Hecht, T.K.-H., Blank, B., Steger, M., Lopez, V., Beck, G., Ramazanov, B., Mann, M., Tagliabracci, V., and von Blume, J. (2020). Fam20C regulates protein secretion by Cab45 phosphorylation. J. Cell Biol. *219*, e201910089.
11. Mitchell, K.J., Tsuboi, T., and Rutter, G.A. (2004). Role for plasma membrane-related Ca2+-ATPase-1 (ATP2C1) in pancreatic beta-cell Ca2+ homeostasis revealed by RNA silencing. Diabetes *53*, 393–400.
12. Kang, T., Boland, B.B., Alarcon, C., Grimsby, J.S., Rhodes, C.J., and Larsen, M.R. (2019). Proteomic Analysis of Restored Insulin Production and Trafficking in Obese Diabetic Mouse Pancreatic Islets Following Euglycemia. J. Proteome Res. *18*, 3245–3258.
13. Rohli, K.E., Boyer, C.K., Bearrows, S.C., Moyer, M.R., Elison, W.S., Bauchle, C.J., Blom, S.E., Yu, C.-L., Pope, M.R., Zhang, J., et al. (2021). Nutrient metabolism regulates insulin granule formation in the pancreatic islet β-cell via ER redox homeostasis. Preprint at bioRxiv. https://doi.org/10.1101/2021.09.22.461417.
14. Honoré, B. (2009). The rapidly expanding CREC protein family: members, localization, function, and role in disease. Bioessays *31*, 262–277.
15. Zhang, Y., Kang, Y.-H., Chang, N., Lam, P.P.L., Liu, Y., Olkkonen, V.M., and Gaisano, H.Y. (2009). Cab45b, a Munc18b-interacting partner, regulates exocytosis in pancreatic beta-cells. J. Biol. Chem. *284*, 20840–20847.
16. Attie Lab Diabetes Database http://diabetes.wisc.edu/.
17. HumanIslets Project https://www.humanislets.com/#/.
18. GTEx Portal https://gtexportal.org/home/gene/SDF4.
19. Le Tissier, P., Fiordelisio Coll, T., and Mollard, P. (2018). The Processes of Anterior Pituitary Hormone Pulse Generation. Endocrinology *159*, 3524–3535.

20. Marengo, F.D., and Cárdenas, A.M. (2018). How does the stimulus define exocytosis in adrenal chromaffin cells? Pflügers Archiv *470*, 155–167.

21. Neher, E. (2018). Neurosecretion: what can we learn from chromaffin cells. Pflügers Archiv *470*, 7–11.

22. Boncompain, G., Divoux, S., Gareil, N., de Forges, H., Lescure, A., Latreche, L., Mercanti, V., Jollivet, F., Raposo, G., and Perez, F. (2012). Synchronization of secretory protein traffic in populations of cells. Nat. Methods *9*, 493–498.

23. Hummer, B.H., Maslar, D., Soltero-Gutierrez, M., de Leeuw, N.F., and Asensio, C.S. (2020). Differential sorting behavior for soluble and transmembrane cargoes at the trans-Golgi network in endocrine cells. Mol. Biol. Cell *31*, 157–166.

24. Sdf4 - 45 kDa calcium-binding protein - Rattus norvegicus (Rat) https://www.uniprot.org/uniprotkb/Q91ZS3/entry.

25. Haataja, L., Snapp, E., Wright, J., Liu, M., Hardy, A.B., Wheeler, M.B., Markwardt, M.L., Rizzo, M.A., and Arvan, P. (2013). Proinsulin intermolecular interactions during secretory trafficking in pancreatic β cells. J. Biol. Chem. *288*, 1896–1906.

26. Boyer, C.K., Bauchle, C.J., Zhang, J., Wang, Y., and Stephens, S.B. (2023). Synchronized proinsulin trafficking reveals delayed Golgi export accompanies β-cell secretory dysfunction in rodent models of hyperglycemia. Sci. Rep. *13*, 5218.

27. Hutton, J.C., Penn, E.J., and Peshavaria, M. (1983). Low-molecular-weight constituents of isolated insulin-secretory granules. Bivalent cations, adenine nucleotides and inorganic phosphate. Biochem. J. *210*, 297–305.

28. Chanat, E., and Huttner, W.B. (1991). Milieu-induced, selective aggregation of regulated secretory proteins in the trans-Golgi network. J. Cell Biol. *115*, 1505–1519.

29. Yoo, S.H., and Lewis, M.S. (1996). Effects of pH and Ca2+ on heterodimer and heterotetramer formation by chromogranin A and chromogranin B. J. Biol. Chem. *271*, 17041–17046.

30. Rossi, A., Pizzo, P., and Filadi, R. (2019). Calcium, mitochondria and cell metabolism: A functional triangle in bioenergetics. Biochim. Biophys. Acta Mol. Cell Res. *1866*, 1068–1078.

31. Genovese, I., Giamogante, F., Barazzuol, L., Battista, T., Fiorillo, A., Vicario, M., D'Alessandro, G., Cipriani, R., Limatola, C., Rossi, D., et al. (2020). Sorcin is an early marker of neurodegeneration, Ca2+ dysregulation and endoplasmic reticulum stress associated to neurodegenerative diseases. Cell Death Dis. *11*, 861.

32. Atakpa-Adaji, P., and Ivanova, A. (2023). IP3R at ER-Mitochondrial Contact Sites: Beyond the IP3R-GRP75-VDAC1 Ca2+ Funnel. Contact *6*, 25152564231181020.

33. Nesselhut, J., Jurgan, U., Onken, E., Götz, H., Barnikol, H.U., Hirschfeld, G., Barnikol-Watanabe, S., and Hilschmann, N. (2001). Golgi retention of human protein NEFA is mediated by its N-terminal Leu/Ile-rich region. FEBS Lett. *509*, 469–475.

34. Skorupska, A., Bystranowska, D., Dąbrowska, K., and Ożyhar, A. (2020). Calcium ions modulate the structure of the intrinsically disordered Nucleobindin-2 protein. Int. J. Biol. Macromol. *154*, 1091–1104.

35. Hur, Y.S., and Yoo, S.H. (2015). Distribution Profile of Inositol 1,4,5-Trisphosphate Receptor/Ca2+ Channels in α and β Cells of Pancreas: Dominant Localization in Secretory Granules and Common Error in Identification of Secretory Granule Membranes. Pancreas *44*, 158–165.

36. Wacquier, B., Combettes, L., and Dupont, G. (2019). Cytoplasmic and Mitochondrial Calcium Signaling: A Two-Way Relationship. Cold Spring Harbor Perspect. Biol. *11*, a035139.

37. Gheni, G., Ogura, M., Iwasaki, M., Yokoi, N., Minami, K., Nakayama, Y., Harada, K., Hastoy, B., Wu, X., Takahashi, H., et al. (2014). Glutamate acts as a key signal linking glucose metabolism to incretin/cAMP action to amplify insulin secretion. Cell Rep. *9*, 661–673.

38. Schuit, F., De Vos, A., Farfari, S., Moens, K., Pipeleers, D., Brun, T., and Prentki, M. (1997). Metabolic fate of glucose in purified islet cells. Glucose-regulated anaplerosis in beta cells. J. Biol. Chem. *272*, 18572–18579.

39. Haythorne, E., Rohm, M., van de Bunt, M., Brereton, M.F., Tarasov, A.I., Blacker, T.S., Sachse, G., Silva Dos Santos, M., Terron Exposito, R., Davis, S., et al. (2019). Diabetes causes marked inhibition of mitochondrial metabolism in pancreatic β-cells. Nat. Commun. *10*, 2474.

40. Lissandron, V., Podini, P., Pizzo, P., and Pozzan, T. (2010). Unique characteristics of Ca2+ homeostasis of the trans-Golgi compartment. Proc. Natl. Acad. Sci. USA *107*, 9198–9203.

41. Rhodes, C.J., and Halban, P.A. (1987). Newly synthesized proinsulin/insulin and stored insulin are released from pancreatic B cells predominantly via a regulated, rather than a constitutive, pathway. J. Cell Biol. *105*, 145–153.

42. Magro, M.G., and Solimena, M. (2013). Regulation of β-cell function by RNA-binding proteins. Mol. Metabol. *2*, 348–355.

43. Norris, N., Yau, B., and Kebede, M.A. (2021). Isolation and Proteomics of the Insulin Secretory Granule. Metabolites *11*, 288.

44. Arvan, P., and Halban, P.A. (2004). Sorting ourselves out: seeking consensus on trafficking in the beta-cell. Traffic *5*, 53–61.

45. Parchure, A., Tian, M., Stalder, D., Boyer, C.K., Bearrows, S.C., Rohli, K.E., Zhang, J., Rivera-Molina, F., Ramazanov, B.R., Mahata, S.K., et al. (2022). Liquid-liquid phase separation facilitates the biogenesis of secretory storage granules. J. Cell Biol. *221*, e202206132.

46. Lara-Lemus, R., Liu, M., Turner, M.D., Scherer, P., Stenbeck, G., Iyengar, P., and Arvan, P. (2006). Lumenal protein sorting to the constitutive secretory pathway of a regulated secretory cell. J. Cell Sci. *119*, 1833–1842.

47. Zhu, Y., Wang, Q., Xu, W., and Li, S. (2008). The ethanol response gene Cab45 can modulate the impairment elicited by ethanol and ultraviolet in PC12 cells. J. Genet. Genomics *35*, 153–161.

48. Seherer, P.E., Lederkremer, G.Z., Uiams, S.W., Fogliano, ∼. M., Baldini, G., and Lodish, H.F. (1996). Cab45, a Novel Ca2+-binding Protein Localized to the Golgi Lumen. J. Cell Biol. *133*, 257–268.

49. Blank, B., and von Blume, J. (2017). Cab45-Unraveling key features of a novel secretory cargo sorter at the trans-Golgi network. Eur. J. Cell Biol. *96*, 383–390.

50. Germanos, M., Gao, A., Taper, M., Yau, B., and Kebede, M.A. (2021). Inside the Insulin Secretory Granule. Metabolites *11*, 515.

51. Pizzo, P., Lissandron, V., Capitanio, P., and Pozzan, T. (2011). Ca(2+) signalling in the Golgi apparatus. Cell Calcium *50*, 184–192.

52. Sharma, R.B., O'Donnell, A.C., Stamateris, R.E., Ha, B., McCloskey, K.M., Reynolds, P.R., Arvan, P., and Alonso, L.C. (2015). Insulin demand regulates β cell number via the unfolded protein response. J. Clin. Invest. *125*, 3831–3846.

53. Evans-Molina, C. (2024). The ailing β-cell in diabetes: Insights from a trip to the ER: The 2023 outstanding scientific achievement award lecture. Diabetes *73*, 545–553.

54. Variant Info https://t2d.hugeamp.org/variant.html?variant=1%3A1163953%3AT%3AC.

55. Newgard, C.B., Lu, D., Jensen, M.V., Schissler, J., Boucher, A., Burgess, S., and Sherry, A.D. (2002). Stimulus/secretion coupling factors in glucose-stimulated insulin secretion: insights gained from a multidisciplinary approach. Diabetes *51*, S389–S393.

56. Zhao, R., Lu, J., Li, Q., Xiong, F., Zhang, Y., Zhu, J., Peng, G., and Yang, J. (2021). Single-cell heterogeneity analysis and CRISPR screens in MIN6 cell line reveal transcriptional regulators of insulin. Cell Cycle *20*, 2053–2065.

57. Tanaka, A., Kosuda, M., Yamana, M., Furukawa, A., Nagasawa, A., Fujishiro, M., Kohno, G., and Ishihara, H. (2023). A large-scale functional analysis of genes expressed differentially in insulin secreting MIN6 sublines with high versus mildly reduced glucose-responsiveness. Sci. Rep. *13*, 5654.

58. Lilla, V., Webb, G., Rickenbach, K., Maturana, A., Steiner, D.F., Halban, P.A., and Irminger, J.-C. (2003). Differential gene expression in well-regulated and dysregulated pancreatic beta-cell (MIN6) sublines. Endocrinology *144*, 1368–1379.

59. Cox, J., and Mann, M. (2008). MaxQuant enables high peptide identification rates, individualized p.p.b.-range mass accuracies and proteome-wide protein quantification. Nat. Biotechnol. *26*, 1367–1372.

60. Schindelin, J., Arganda-Carreras, I., Frise, E., Kaynig, V., Longair, M., Pietzsch, T., Preibisch, S., Rueden, C., Saalfeld, S., Schmid, B., et al. (2012). Fiji: an open-source platform for biological-image analysis. Nat. Methods *9*, 676–682.

61. Tyanova, S., Temu, T., Sinitcyn, P., Carlson, A., Hein, M.Y., Geiger, T., Mann, M., and Cox, J. (2016). The Perseus computational platform for comprehensive analysis of (prote)omics data. Nat. Methods *13*, 731–740.

62. Seidah, N.G., Benjannet, S., Wickham, L., Marcinkiewicz, J., Jasmin, S.B., Stifani, S., Basak, A., Prat, A., and Chretien, M. (2003). The secretory proprotein convertase neural apoptosis-regulated convertase 1 (NARC-1): liver regeneration and neuronal differentiation. Proc. Natl. Acad. Sci. USA *100*, 928–933.

63. Harney, D.J., Cielesh, M., Roberts, G.E., Vila, I.K., Viengkhou, B., Hofer, M.J., Laguette, N., and Larance, M. (2023). Dietary restriction induces a sexually dimorphic type I interferon response in mice with gene-environment interactions. Cell Rep. *42*, 112559.

STAR★METHODS

KEY RESOURCES TABLE

REAGENT or RESOURCE	SOURCE	IDENTIFIER
Antibodies		
Cab45G (rabbit polyclonal)	Laboratory of Julia von Blume	N/A
Insulin (guinea pig polyclonal)	Agilent DAKO	Cat# IR00261-2, RRID:AB_2800361
Proinsulin GS-9A8 (mouse monoclonal)	Developmental Studies Hybridoma Bank	RRID: AB_532383
TGN38 (mouse monoclonal)	Novus Biologicals	Cat# NB300-575; RRID: AB_2240559
GM130 (mouse monoclonal)	BD Biosciences	Cat# 610822; RRID:AB_398141
Glucagon (mouse monoclonal)	Sigma	Cat# G2654; AB_259852
HA C29F4 (rabbit polyclonal)	Cell Signaling	Cat# 3724; RRID:AB_1549585
β-Actin (mouse monoclonal)	Sigma	Cat# A5441; RRID:AB_476744
Chemicals, peptides, and recombinant proteins		
Fura-AM	Thermo Fisher	F1221
Lipofectamine 2000	Thermo Fisher	11668027
Critical commercial assays		
Rat Insulin ELISA kit	Mercodia	10-1113-01
Rat proinsulin ELISA kit	Mercodia	10-1118-01
Pierce BCA Protein Assay Kit	Thermo Fisher	23225
Quant-iT PicoGreen dsDNA Assay	Thermo Fisher	P7589
Deposited data		
INS1 Cab45KO cell proteome – raw data	This paper	Deposited on ProteomeXchange Consortium (https://proteomecentral.proteomexchange.org/ui), accession PXD052042.
Experimental models: Cell lines		
INS1 cells	Laboratory of Cedric Asensio	INS-1 (RRID:CVCL_0352)
INS1 Cab45KO cells	Laboratory of Cedric Asensio	N/A
Oligonucleotides		
RUSH plasmid – Cab45-GFP-SBP	This paper	N/A
LentiCRISPR-v2 containing gRNA forward: 5' – CTGTGGTCTGGCTG CTCATG – 3'; reverse: 5′ CATGAG CAGCCAGACCACAG – 3′	This paper	N/A
CRISPR/Cas9 pX330 containing gRNA targeting exon 2 Forward-5′-3':CTGTGGTCTGGCTGCTCATG; Reverse-5′-3':CATGAGCAGCCA GACCACAG	This paper	N/A
Software and algorithms		
GraphPad Prism 9	N/A	https://www.graphpad.com/
MaxQuant	Cox and Mann 2008[59]	https://www.maxquant.org/
ImageJ (FIJI)	Schindelin et al. 2012[60]	https://imagej.net/software/fiji/
Perseus	Tyanova et al. 2016[61]	https://www.maxquant.org/perseus/

EXPERIMENTAL MODEL AND STUDY PARTICIPANT DETAILS

Human pancreas tissue

Fixed, paraffin-embedded, pancreas tissue sections were provided by St. Vincent's Institute of Medical Research (Victoria, Australia) with informed consent from next of kin and human research ethics committees approval (HREC-2017/042). 8 non-diabetic donors

and 7 type 2 diabetic-donor pancreas tissue samples were used in this study. Subjects were grouped/allocated solely by diabetic status. Additional donor information including age, sex, BMI, HbA1c, diabetes duration, and glucose-lowering therapy usage can be found in Table S1. Human pancreas donor information, related to Figures 1 and 2.

Rat insulinoma INS1 cell lines

Rat INS1 cell lines (sex: male) obtained from collaborator Dr. Cedric Asensio were cultured at 37°C and 5% CO2 in RPMI 1640 Medium (Gibco) containing 11 mM glucose, 2.05 mM L-Glutamine, 10% FBS, 10 mM HEPES, 1 mM Sodium Pyruvate, 0.05 mM 2-β-mercaptoethanol and 1% penicillin-streptomycin. The cell line has not been authenticated since original receipt from collaborator Peter Arvan, and cells were shown to be mycoplasma free by DAPI staining and PCR test (ABM, G238).

Cab45KO INS1 cells

Cab45KO INS1 cells were produced by transfection with lentiCRISPR-v2 and a CRISPR/Cas9 pX330 vector containing gRNA targeting exon 2 (Forward-5′-3':CTGTGGTCTGGCTGCTCATG; Reverse-5′-3':CATGAGCAGCCAGACCACAG). INS1e cells were transfected with lentiCRISPR v2 and a CRISPR/Cas9 pX330 vector containing gRNA (forward: 5' – CTGTGGTCTGGCTGCTCATG – 3'; reverse: 5′ CATGAGCAGCCAGACCACAG – 3′) that targets exon 2 of Cab45/*SDF4*. 24 h after transfection, cells were treated transiently with 2 μg/mL of puromycin (Goldbio, CAT# p-600-100) to select for transfected cells. Single clones from the resulting population of cells were plated in a round bottom 96-well plate. A population of single clones with Cab45 KO were used for experiments.

METHOD DETAILS

In situ hybridization

In situ hybridisation of *SDF4* mRNA was conducted as described previously.[62] Briefly, antisense and sense mRNA probes generated for *SDF4* were labeled with 35^S-UTP and 35^S-CTP. Mice were sacrificed either at embryonic stages e10, e12 and e15, postnatal stages p1 and p5, or in adult mice. Hybridisation of probes was conducted overnight at 55°C on 8–10 μm tissue cryostat sections that had been fixed with 4% paraformaldehyde (PFA). For autoradiography, sections were dipped in photographic emulsion and exposed for 6–12 days, and also stained with cresyl violet for more imaging.

Pancreas immunofluorescence staining

Paraffin-embedded human pancreas sections were deparaffinized and rehydrated through a xylene and ethanol series. Sections were washed in wash buffer (0.1% BSA in PBS with 0.01% sodium azide) before cell permeabilization in Dako Target Retrieval Solution (Agilent). Non-specific binding was blocked for 1 h at room temperature (RT) using Dako Protein Block Serum-Free (Agilent) after washing, then sections were incubated with primary antibodies in Dako Antibody Diluent (Agilent) overnight at 4°C. Sections were washed then incubated with appropriate Alexa Fluor secondary antibodies (Thermo Fisher Scientific) in Dako Antibody Diluent for 1 h at RT. Coverslips were mounted onto glass slides using Prolong Diamond Antifade Mountant (Thermo Fisher Scientific) with/without DAPI, and imaged with a Leica SP8 confocal microscope.

INS1 immunofluorescence staining

INS1 cells plated on coverslips were washed with PBS twice before fixing with 4% paraformaldehyde at RT for 20 min. Fixed cells were washed twice with PBS, twice with wash buffer (0.1% BSA in PBS with 0.01% sodium azide), then treated with 0.1% SDS for 5 min at RT to permeabilize cell membranes. Non-specific binding was blocked with Dako Protein Block Serum Free for 1 h at RT. Cells were incubated with primary antibodies in Dako Antibody Diluent overnight at 4°C. Cells were washed twice in wash buffer for 3 min with shaking, then incubated with fluorophore-conjugated secondary antibodies in Dako Antibody Diluent for 1 h at RT. Coverslips were mounted into glass slides using Prolong Diamond Antifade Mountant with/without DAPI and imaged with a Leica SP8 confocal microscope using Leica LAS X software, or an Olympus Fluoview FV1200 confocal microscope with a 60× UPlanSApo oil objective (numerical aperture = 1.35) using Olympus Fluoview v4.2 acquisition software.

Transient DNA transfection

Transient transfections were performed on seeded INS1 cells in 6-well plates using 0.5 μg of pLPCX retroviral expression vectors, generated by collaborator Julia von Blume as described,[9] with 10 μL Lipofectamine 2000 (Thermo Fisher) in 2 mL OptiMEM (Gibco) for 6 h. Cells were then cultured for 48 h in RPMI-1640.

Cell harvest and immunoblotting

Confluent cells were washed with ice-cold PBS, gently scraped into tubes, and centrifuged at 1000 rpm for 3 min. The supernatant was aspirated and cells resuspended in RIPA buffer (Thermo Fisher Scientific) supplemented with EDTA-free protease inhibitors (Roche). Cells were lysed by sonication then centrifuged at 12 000 x g for 15 min, and lysate transferred to a fresh tube. Protein concentrations were quantified using the Pierce BCA Protein Assay Kit (Thermo Fisher Scientific). Proteins in whole-cell lysates were separated using Tris/glycine-SDS-PAGE under denaturing conditions in 10% polyacrylamide gels, then transferred to methanol-activated PVDF membranes.

Retention using selective hooks (RUSH)

RUSH plasmid generation

To produce the RUSH plasmid expressing Cab45-GFP-SBP, Cab45 was first amplified from rat cDNA using forward 5' – ATATTCTAGACCACCATGGTCTGGCTGGCGGCA – 3′ and reverse 5' – ATATGGATCCCTCGAGTTAGAACTCTTCATGCACATTGC GG - 3′ primers. The product was ligated into a pLenti-puro backbone cut with Xba1 and BamH1. Forward primer 5' – ATATACC GGTCCACCATGGTCTGGCTGGCGGCA – 3′ and reverse primer 5' –ATATAAGCTTGAACTCTTCATGCACATTGCGG – 3′ was used to amplify Cab45G, and the product was ligated into a pEGFP backbone containing GFP-SBP after being cut with Age1 and HindIII.

RUSH cell culture and transfection

INS1 cells were cultured in RPMI 1640 (Genesee Scientific, Cat# 25-506H) with 10% fetal bovine serum (VWR, Cat#89510-186) and 1 mM sodium pyruvate (Genesee Scientific, Cat#25–537) in 5% CO^2 at 37°C. Cells were seeded in a 24-well dish at 40–60% confluency and transfected with Fugene HD (Promega, Cat#E2311) according to the manufacturer protocol with a 3:1 M ratio of hook to cargo plasmid and 100 ng of a TGN marker. 24 h following transfection, cells were trypsinized and moved to a 35 mm glass bottom cell culture dish (VWR, Cat#75856-744) and imaged 36–48 h after transfection.

RUSH video acquisition and processing

Live movies were imaged on an Evos FL Auto 2 in an environmentally controlled imaging chamber (37°C, 5% CO_2, 20% humidity). Cells were imaged every 2 min. Image processing was performed using MATLAB software. To isolate regions of interest, each frame of the Golgi-labeled channel was manually cropped around the general cell area and segmented using an intensity threshold filter. The segmented region of interest was constrained by an area filter to reduce noise, generating a binary mask of only the largest objects within the frame. The mask was then convoluted with the cargo channel to obtain the TGN signal. For figures, images were processed using ImageJ, any changes in brightness and contrast were identical between samples meant for comparison. K_{ER} and K_{TGN} curves were fit using a first order decay curve found in GraphPad Prism version 8.0.2 for Windows, GraphPad Software, La Jolla California (USA). K_{TGN} was fit using plateau followed by one phase decay with a constraint that X0 is greater than 0 and K_{ER} was fit using first order decay.

Transmission electron microscopy

INS1 cells were cultured on ThermanoxTM coverslips, then fixed and prepared for sectioning; silver-gold ultrathin sections (~70 nm) were generated using a Leica EM UC7 ultramicrotome (Leica, Heerbrugg, Switzerland), then mounted onto 200-mesh copper grids (G200-Cu, Electron Microscopy Sciences, Hatfield, PA, USA). Post-staining was performed using an aqueous solution of 2% uranyl acetate for 10 min, followed by Reynold's lead citrate for 10 min. Stained sections were viewed using a JEOL 1400 TEM (Tokyo, Japan) operating at 120 kV. Across three experiments, total ISG and MSG were counted in 9–11 cell images per control and Cab45KO INS1 samples. Samples from EM data were processed and imaged blinded by the Australian Microscopy and Microanalysis Facility, University of Sydney.

Mass spectrometry-based proteomics

Sample digestion and processing

INS1 lysates obtained by boiling in 4% sodium deoxycholate (SDC) containing 100 mM Tris-HCl (pH 8.0) for 10 min at 95°C and subjection to water-bath sonication (10 min total sonication time, 30 s on/off, 20% amplitude, QSonica Q800R2) and centrifugation (18,000 g, 10 min, 18°C). Protein digestion and LC-MS/MS analysis was performed as described[63] but with modifications.

Mass spectrometry-based analysis

Analysis was performed using either Q exactive HF or Fusion Lumos tribrid mass spectrometer (Thermo Fisher) with higher-energy collisional dissociation (NCE = 30). MS/MS spectra were attained in a data-dependent acquisition of the top 20 most abundant ions in each MS1 full scan. Raw data have been deposited to the ProteomeXchange Consortium (https://proteomecentral.proteomexchange.org/ui) via PRIDE partner repository with dataset identifier PXD052042 (Username:reviewer_pxd052042@ebi.ac.uk; Password:LfkBjJsU). RAW data files were analyzed using integrated quantitative proteomics software and MaxQuant (version 1.6.14.0). A false discovery rate of 1% using a target-decoy based strategy was used for protein and peptide identification. The database used for identification contained both Uniprot rat Swissprot and Trembl databases alongside the MaxQuant contaminants database. Mass tolerance: 4.5 ppm for precursor ions and 20 ppm for fragments. Digestion enzyme: Trypsin with maximum 2 missed cleavages. Variable modifications: oxidation of Met, deamidation of Asn/Gln, pyro-Glu/Gln, and protein N-terminal acetylation. Fixed modification: Carbamidomethylation of Cys. The MaxLFQ algorithm was used for label-free quantification.

Glucose-stimulated insulin secretion (GSIS)

GSIS was assessed as previously described,[4] with modifications. INS1 cells cultured in 6-well plates were starved overnight in a low-glucose RPMI 1640 (GibcoTM) containing 2.8 mM glucose, 2.05 mM L-glutamine, 10% FBS, 10 mM HEPES, 1 mM sodium pyruvate, 0.05 mM 2-β-mercaptoethanol. The following day, media was replaced with a Krebs buffer (20 mM HEPES, pH 7.4, 119 mM NaCl, 4.75 mM KCl, 2.54 mM $CaCl_2$, 1.2 mM $MgSO_4$, 1.18 mM KH_2PO_4, 5 mM $NaHCO_3$, 0.5% BSA) containing 2.8 mM glucose for 1 h (basal). Following this, the media was replaced with 2.8 mM glucose Krebs buffer or 16.7 mM glucose for 1 h. Repeated challenge of insulin secretion was performed by including an additional 30 min incubation in 2.8 mM glucose followed by 16.7 mM glucose for 1

h. Media was collected to measure insulin secretion by HTRF assay (CisBio Assay). Cells were collected in Islet Lysis buffer (100 mM Tris, 300 mM NaCl, 10 mM NaF, 2 mM Na_3VO_4, and protease inhibitors) and sonicated to measure insulin content by HTRF assay and DNA content with the Quant-iT PicoGreen dsDNA Assay kit (Thermo Fisher Scientific). For a subset of insulin secretion experiments presented in Figure S3, GSIS was performed the same as above except that the cells were rested at 2.8 mM glucose for 1 h and not overnight before stimulation with either 2.8 mM or 16.7 mM glucose. Insulin and proinsulin were measured using two different specific ELISA assay kits (Mercodia).

Ca^{2+} depletion in INS1 cells

INS1 cells were incubated in Ca^{2+}-free media (140 mM NaCl, 5 mM KCl, 1 mM $MgCl_2$, 5 mM $NaHCO_3$, 10 mM HEPES, pH 7.4) for 20 min before treatment with 5 μM ionomycin and 5 mM EGTA.

Ca^{2+} imaging with Fura-2 a.m

INS1 cells cultured at 50–60% confluency in 35 mm Mattek glass bottom dishes (No. 1.5 coverslip) were starved overnight in a low glucose RPMI 1640 (GibcoTM) containing 2.8 mM glucose, 2.05 mM L-glutamine, 10% fetal bovine serum (FBS), 10 mM HEPES, 1 mM sodium pyruvate, 0.05 mM 2-β-mercaptoethanol. The next day, cells were washed in ECB (2.5 mM $CaCl_2$, 140 mM NaCl, 5 mM KCl, 1 mM $MgCl_2$, 5 mM $NaHCO_3$, and 10 mM HEPES, pH 7.4), and then incubated for 30 min with ECB, containing 2.8 mM glucose, 4 μM Fura-2a.m., and 0.02% pluronic acid. Cells were then incubated for a further 30 min in ECB containing 1% pluronic acid to enhance dye loading. Imaging was performed using a Nikon Eclipse Ti-E spinning disc confocal microscope, housed in a live-cell imaging chamber. The chamber conditions were 37° C and 5% CO_2. Cells were excited alternately with light at 340 and 380 nm every 50 ms using a Lambda DG-4 Xenon high-speed wavelength switcher (Sutter Instruments). Fura-2 a.m.-loaded INS1 cells were first imaged for 3 min in a 2.8 mM glucose ECB to measure resting Ca^{2+}, before addition of 16.7 mM glucose and acquisition of Ca^{2+} oscillations for 45 min. Following glucose stimulation, ECB containing 40 mM KCl (105 mM NaCl, 40 mM KCl, 1 mM $MgCl_2$, 5 mM $NaHCO_3$, 10 mM HEPES, pH 7.4) was added to depolarize cell membranes. A single calibration trace was recorded by depleting cells of Ca^{2+} using a zero Ca^{2+} ECB (142.5 mM NaCl, 5 mM KCl, 1 mM $MgCl_2$, 5 mM $NaHCO_3$, 10 mM HEPES, pH 7.4) containing 1 mM ionomycin and 5 mM EGTA, followed by 3 washes with ECB to remove EGTA, and then incubation of cells in high Ca^{2+} ECB (10 mM $CaCl_2$, 132.5 mM NaCl, 5 mM KCl, 1 mM $MgCl_2$, 4 mM $NaHCO_3$, 10 mM HEPES, pH 7.4) containing 1 mM ionomycin to flood cells with Ca^{2+}. Recordings were analyzed using NIS-Elements software (Nikon) to draw regions of interest around cells and extract fluorescent traces. Statistical analyses were performed using Microsoft Excel and GraphPad Prism 9. Fura-2 recordings were calibrated for intracellular [Ca^{2+}] using the Tsien formula.

QUANTIFICATION AND STATISTICAL ANALYSIS

Analyses were performed using FIJI (ImageJ), NIS-Elements (Nikon), Perseus (MaxQuant), and Prism 9 (GraphPad). Statistical analyses were performed using GraphPad Prism 9 software. Statistical significance was determined by two-tailed Student's t test, one-way ANOVA or two-way ANOVA with Tukey's multiple comparisons post-test corrected for multiple comparisons. Relevant *n*-values, dispersion and precision measures, statistical tests and significance values are indicated within the figure legends or within graphs of corresponding data. Parametric tests were performed unless indicated, where Gaussian distribution was determined by normality test. A value of $p < 0.05$ was considered significant.